KeAi
CHINESE ROOTS
GLOBAL IMPACT

Contents lists available at ScienceDirect

# Petroleum Science





# Original Paper

# Effect of cyclic hydraulic stimulation on pore structure and methane sorption characteristics of anthracite coal: A case study in the Qinshui Basin, China



Rui-Shuai Ma <sup>a, b, c</sup>, Ji-Yuan Zhang <sup>a, b, c, \*</sup>, Qi-Hong Feng <sup>b, c, d</sup>, Xue-Ying Zhang <sup>e</sup>, Yan-Hui Yang <sup>f</sup>

- a State Key Laboratory of Deep Oil and Gas, China University of Petroleum (East China), Qingdao, 266580, Shandong, PR China
- <sup>b</sup> School of Petroleum Engineering, China University of Petroleum (East China), Qingdao 266580, Shandong, PR China
- <sup>c</sup> Key Laboratory of Unconventional Oil & Gas Development (China University of Petroleum (East China)), Ministry of Education, Qingdao 266580, Shandong, PR China
- <sup>d</sup> Shandong Institute of Petroleum and Chemical Technology, Dongying, 257000, Shandong, PR China
- <sup>e</sup> PetroChina Research Institute of Petroleum Exploration & Development, Beijing 100083, PR China
- f PetroChina Huabei Oilfield Company, Renqiu, 062552, Hebei, PR China

#### ARTICLE INFO

# Article history: Received 24 December 2023 Received in revised form 3 August 2024 Accepted 7 August 2024 Available online 8 August 2024

Edited by Yan-Hua Sun

Keywords:
Coalbed methane
Cyclic hydraulic stimulation
Pore structure
Methane sorption characteristics
Fractal analysis

#### ABSTRACT

The cyclic hydraulic stimulation (CHS) has proven as a prospective technology for enhancing the permeability of unconventional formations such as coalbeds. However, the effects of CHS on the microstructure and gas sorption behavior of coal remain unclear. In this study, laboratory tests including the nuclear magnetic resonance (NMR), low-temperature nitrogen sorption (LTNS), and methane sorption isotherm measurement were conducted to explore changes in the pore structure and methane sorption characteristics caused by CHS on an anthracite coal from Qinshui Basin, China. The NMR and LTNS tests show that after CHS treatment, meso- and macro-pores tend to be enlarged, whereas micropores with larger sizes and transition-pores may be converted into smaller-sized micro-pores. After the coal samples treated with 1, 3, 5 and 7 hydraulic stimulation cycles, the total specific surface area (TSSA) decreased from 0.636 to 0.538, 0.516, 0.505, and 0.491 m<sup>2</sup>/g, respectively. Fractal analysis based on the NMR and LTNS results show that the surface fractal dimensions increase with the increase in the number of hydraulic stimulation cycles, while the volume fractal dimensions exhibit an opposite trend to the surface fractal dimensions, indicating that the pore surface roughness and pore structure connectivity are both increased after CHS treatment. Methane sorption isothermal measurements show that both the Langmuir volume and Langmuir pressure decrease significantly with the increase in the number of hydraulic stimulation cycles. The Langmuir volume and the Langmuir pressure decrease from 33.47 cm<sup>3</sup>/ g and 0.205 MPa to 24.18 cm<sup>3</sup>/g and 0.176 MPa after the coal samples treated with 7 hydraulic stimulation cycles, respectively. The increments of Langmuir volume and Langmuir pressure are positively correlated with the increment of TSSA and negatively correlated with the increments of surface fractal dimensions. © 2024 The Authors. Publishing services by Elsevier B.V. on behalf of KeAi Communications Co. Ltd. This is an open access article under the CC BY-NC-ND license (http://creativecommons.org/licenses/by-nc-nd/ 4.0/).

# 1. Introduction

The capture or development of coalbed methane (CBM) from coalbeds has multiple favorable effects such as enhancing the underground coal mining activity safety, adding to global natural gas supply, and reducing the emission of methane into the atmosphere (Li et al., 2023; Liang et al., 2023; Tao et al., 2019). To date, the commercial development of CBM has been undertaken worldwide, including the United States, China, Australia, and India (Li et al., 2024a; Senthamaraikkannan et al., 2016). In China, the CBM industrialization bases have been successfully established in the Qinshui and Ordos basins (Su et al., 2020), where the majority of CBM reservoirs are characterized by ultra-low permeability, low in-

<sup>\*</sup> Corresponding author. State Key Laboratory of Deep Oil and Gas, China University of Petroleum (East China), Qingdao 266580, Shandong, PR China. E-mail address: zhjy221@126.com (J.-Y. Zhang).

situ pressure, and high stress (Cao et al., 2016; Li A. et al., 2018). To achieve economically viable gas production, hydraulic stimulation technology has been widely applied in these regions (Li et al., 2024a, 2024b). However, field applications showed that the conventional hydraulic stimulation technology typically results in relatively simple hydraulic fractures rather than complex fracture network (Cheng et al., 2018), which leads to low gas production and low recovery factor of CBM wells (Ni et al., 2019). Moreover, conventional hydraulic stimulation technology requires the injection of a large amount of water, which may induce the effect of local stress concentration and thus result in earthquakes (DiStefano et al., 2019). Hence, the search for hydraulic stimulation technologies with higher CBM recovery factor and lower seismic activity has drawn significant attention (Gaucher et al., 2015; Lee et al., 2019).

The cyclic hydraulic stimulation (CHS) technology has proven to be a promising technology for improving hydrocarbon recovery in low-permeable reservoirs (Rutqvist et al., 2007; Velcin et al., 2020). The basic philosophy of the CHS is to inject fracturing fluid into the reservoir with small amounts and multiple times. The cyclic injection results in an action of alternating loads on the reservoir rocks, which is favorable to the propagation of tensor-shear fractures and tends to produce more complex fracture networks (Tang et al., 2020). Recently, numerous studies have been undertaken to investigate the formation and propagation of macroscopic hydraulic fractures under the action of CHS. Wang et al. (2015) explored the formation mechanism of alternating loads in the CHS process, and observed a 2.6-fold increase in the total amount of CBM compared to conventional hydraulic stimulation. Patel et al. (2017) found that the damage to the rocks surrounding hydraulic fractures caused by CHS technology is approximately twice as extensive as that resulting from conventional hydraulic stimulation methods. AlTammar and Sharma (2019) reported the impact of CHS on breakdown pressure. Their results indicate that CHS has the potential to reduce breakdown pressure, thereby facilitating the formation of hydraulic fractures. Besides, some scholars have conducted a comparison of seismic waves between samples subjected to conventional hydraulic stimulation treatment and those treated with CHS (Ji et al., 2021; Niemz et al., 2020). The experimental results indicate that the application of CHS promotes the diffusion of fluid pressure along the faults, reduces the heterogeneity of fluid pressure distribution and the frequency of high-magnitude seismic events. In conclusion, CHS technology has demonstrated promising prospects for reducing seismicity and enhancing the coalbeds permeability in CBM extraction.

However, coal is generally regarded as a dual-porosity medium, composing both matrix and cleat systems (Hu et al., 2023; Mohanty and Kumar, 2017). The micro-pores in the matrix present a strong affinity for CBM, with approximately 90%—98% of CBM stored in an adsorbed state within these pores (Yang et al., 2019). The sorption characteristics of coal determine the amount of CBM migration from the matrix to the cleat system, playing a crucial role in the production of CBM. In the process of reducing potential seismic risks and enhancing coal seam permeability by CHS technology, there is an inevitable impact on the microscopic pore structure of coal, thereby changing the methane sorption characteristics of coal. Thus, a comprehensive grasp of the impact of CHS on coal pore structure and methane sorption characteristics is vital for the development and utilization of CBM.

Unfortunately, to date, scholars have paid limited attention to the changes in coal pore structure and methane sorption characteristics after CHS treatment. In this study, nuclear magnetic resonance (NMR) testing, low-temperature nitrogen sorption (LTNS) analysis, and fractal theory were employed to assess the changes in microstructure of coal. Additionally, methane sorption isotherm measurements were carried out to clarify the effects of CHS on the

sorption characteristics of coal. Combining these tests and analyses, this study reveals the mechanisms underlying the changes in microstructure and sorption characteristics induced by CHS in anthracite coal from the Qinshui Basin.

#### 2. Method

#### 2.1. Sample collection

The coal samples were taken from the Sihe coal mine located in the southern margin of the Qinshui Basin, China. All the coal samples were directly collected from the fresh workface of the underground tunnel. Coal samples were wrapped in plastic immediately after retrieval, and promptly transported to the laboratory for further analysis. Table 1 provides analytical details of the coal samples, including the elemental and proximate analyses. According to Chinese classification of coals (GB/T 5751-2009), the volatile matter content of the collected coal samples is less than 10%, indicating that the collected coal samples belong to anthracite coal. Additionally, it can be seen from Table 1 that the proportion of magnetic minerals (such as Fe) is less than 0.25%. It means that the impact of magnetic minerals in the collected coal samples on the NMR results can be neglected (Sun et al., 2021; Zheng et al., 2019).

# 2.2. Sample preparation and CHS treatment

This paper integrates three groups of experiments, namely CHS treatment, pore structure characterization (NMR and LTNS testing). and methane sorption isotherm measurements. The CHS treatment experiments were conducted by the ZYB-II vacuum watersaturating system (Unipac, China). It comprises a high-pressure vessel with the size of  $\Phi$ 120 mm  $\times$  300 mm, a vacuum pump with a maximum vacuum of  $6 \times 10^{-2}$  Pa and a hand pump with a maximum working pressure of 30 MPa. The coal samples were divided into five groups for representing different CHS treatment conditions: untreated samples (reference group), samples treated with 1 hydraulic stimulation cycle, samples treated with 3 hydraulic stimulation cycles, samples treated with 5 hydraulic stimulation cycles, and samples treated with 7 hydraulic stimulation cycles. In this study, the CHS treatment pressure was set at 18 MPa, referencing the operational pressure in the Qinshui Basin. Moreover, to mitigate the impact of CHS treatment time on experimental results, a consistent total treatment duration was maintained for each sample. The CHS treatment process of coal samples is shown in Fig. 1.

To meet the sample size requirements for different types of experimental, cylindrical coal samples and coal particles were prepared, respectively. The preparation steps of coal samples are as follows: 1) Cylindrical coal samples with a length of 50 mm and a diameter of 25 mm were drilled from a large coal block for CHS treatment and NMR testing. 2) Four groups of standard columnar coal samples with similar  $T_2$  spectra were selected before CHS treatment to reduce the impact of the heterogeneity of coal samples on the NMR results (the selection result is supplied in Appendix A). 3) The coal fragments near the cylindrical coal samples were collected and crushed into particles, then the coal particles were sieved to 60-80 mesh for subsequent CHS treatment, LTNS analysis, and methane sorption isotherm measurements.

# 2.3. Pore structure and methane sorption characteristic characterization methods

# 2.3.1. NMR analysis

NMR testing was conducted by MacroMR12-150H-VTHP low-field NMR device (Niumag, China). The magnetic field intensity,

R.-S. Ma, J.-Y. Zhang, Q.-H. Feng et al. Petroleum Science 21 (2024) 3271–3287

**Table 1**Basic properties of the coal samples.

Proximate analysis				Elemental analysis						
M <sub>ad</sub> , %	A <sub>d</sub> , %	V <sub>d</sub> , %	FC <sub>ad</sub> , %	C, %	Н, %	N, %	0, %	S, <b>%</b>	Others, %	
1.16	12.95	9.84	78.48	91.27	3.44	1.35	3.38	0.31	0.25	

Notes:  $M_{ad}$  and  $FC_{ad}$  represent moisture and fixed carbon on air-dried base;  $A_d$  and  $V_d$  are ash and volatile matter on dry basis.

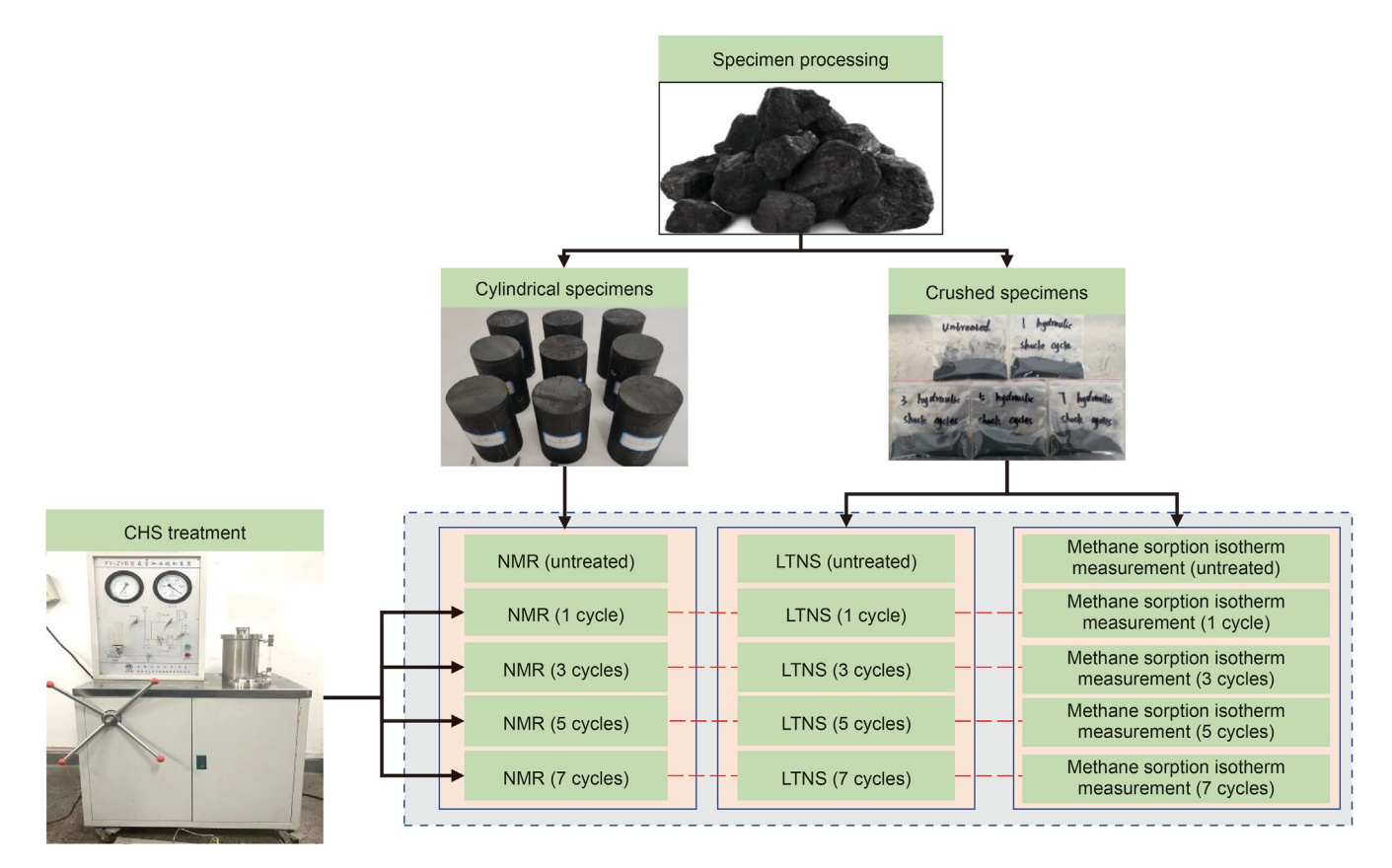


Fig. 1. CHS treatment process of coal samples.

main frequency, and maximum sampling bandwidth of the equipment are 0.05 T, 12.8 MHz and 2000 kHz, respectively. NMR employs a mechanism to characterize pore structure by measuring the relaxation signal of hydrogen atoms within coal pores and fractures. The correlation between the transverse relaxation time ( $T_2$ ) and the pore radius is utilized to reveal the pore structure, and the relationship between the  $T_2$  and the pore radius is as follows (Chen et al., 2023):

$$\frac{1}{T_2} = \frac{\rho}{r} F_{\mathsf{S}} \tag{1}$$

where  $T_2$  is the transverse relaxation time, ms;  $\rho$  is the surface relaxation rate, nm/ms;  $F_s$  is the pore shape factor; r is the pore radius, nm. In this study,  $F_s = 2$ , the calculation result for  $\rho$  is 17.98 nm/ms (the calculation process is supplied in Appendix B).

# 2.3.2. LTNS analysis

LTNS analysis was performed using Micromeritics ASAP 2020M system with the test temperature and relative pressure are  $-196\,^{\circ}\text{C}$  and 0-0.99, respectively. Before LTNS analysis, all samples were dried at 381 K in a vacuum oven for 24 h. The specific surface area (SSA) and pore volume (PV) were calculated with the BET and the

BJH models (Han et al., 2022), respectively.

# 2.3.3. Methane sorption isotherm measurements

Before methane sorption isotherm measurements, all samples (the reference group and CHS treatment groups) were dried at 381 K in a vacuum oven for at least 48 h until the change in the sample mass is within ±0.001 g. This procedure is to remove the injected water out of the coal samples, thereby minimizing the effect of moisture on the methane sorption isotherm measurements. The sorption amount was tested using the manometric method (Bush and Gensterblum, 2011) for all samples at a constant temperature of 303 K. The measured sorption amount was fitted using the Langmuir model in order to quantitatively evaluate the impact of CHS on the methane sorption characteristics. The Langmuir model is expressed as follows (Huang et al., 2019; Sudibandriyo et al., 2003):

$$V_{abs} = \frac{V_{L}P}{(P_{L} + P)(1 - \rho_{g}/\rho_{s})}$$
 (2)

where  $V_{\rm abs}$  is the absolute sorption amount, mL/g;  $V_{\rm L}$  is the Langmuir volume, mL/g;  $P_{\rm L}$  is the equilibrium pressure, MPa;  $P_{\rm L}$  is the Langmuir pressure, MPa;  $\rho_{\rm g}$  is the density of methane for free

phase,  $g/cm^3$ ;  $\rho_s$  is the density of methane for sorption phase,  $g/cm^3$ , it can be regard as a constant of 0.421  $g/cm^3$ .

# 3. Results and analysis

### 3.1. NMR analysis

## 3.1.1. $T_2$ spectra analysis

Fig. 2 illustrates the  $T_2$  spectra of the coal samples before and after CHS treatment. The  $T_2$  spectra of the tested coal samples exhibit similar pattern, displaying a trimodal distribution characterized with three distinct peaks in the regions of 0.01-10, 10-100, and 100-10000 ms, respectively. Moreover, it can also be seen from Fig. 2 that both the peak value and span of peaks 2 and 3 (P2 and P3) present an increase trend with the increase of CHS treatment cycles. It indicates that after CHS treatment, not only the pores corresponding to P2 and P3 are expanded, but also some new pores are generated. However, after CHS treatment, the  $T_2$  spectra of peak 1 (P1) for all samples shifted diagonally to the left. The results suggest that the expansion and generation of pores corresponding to P2 and P3 may compress the pores corresponding to P1. Furthermore. before and after CHS treatment, there is an intersection point  $(T_p)$ for P1, which can divide P1 into two segments. When the  $T_2$  value of P1 is less than  $T_p$ , the  $T_2$  spectra of the coal samples treated with CHS are above those before CHS treatment, indicating that both the

porosity and the number of pores in this region are increased after CHS treatment. When the  $T_2$  value of the P1 is greater than  $T_p$ , the  $T_2$  spectra of coal samples treated with CHS are lower than those before CHS treatment, indicating that both the porosity and the number of pores in this region are decreased after CHS treatment. The results suggest that CHS does not uniformly compress all corresponding pores of P1; instead, it selectively compresses some larger pores into smaller ones. Additionally, after 1, 3, 5, and 7 hydraulic stimulation cycles, the  $T_p$  values were 0.594, 0.542, 0.508, and 0.493 ms, respectively, showing a decreasing trend with an increase in hydraulic stimulation cycles. This trend indicates that the increase in the number of hydraulic stimulation cycles enhances the compressive effect on larger pores corresponding to P1.

### 3.1.2. PSD analysis based on NMR

Pores in coals can be classified into four categories according to the pore size, namely the micro-pores (< 10 nm), transition-pores (10–100 nm), meso-pores (100–1000 nm) and macro-pores (> 1000 nm) (Hodot, 1961). To clarify the changes in PSD for all pore types before and after CHS treatment, the PSD curves of all tested coal samples obtained from NMR were segmented. Fig. 3 illustrates that the PSD curves exhibit distinct trends for different pore types after CHS treatment. For meso- and macro-pores, the height and span of the PSD curves for coal samples treated with CHS are larger than those of the untreated coal samples, suggesting that CHS

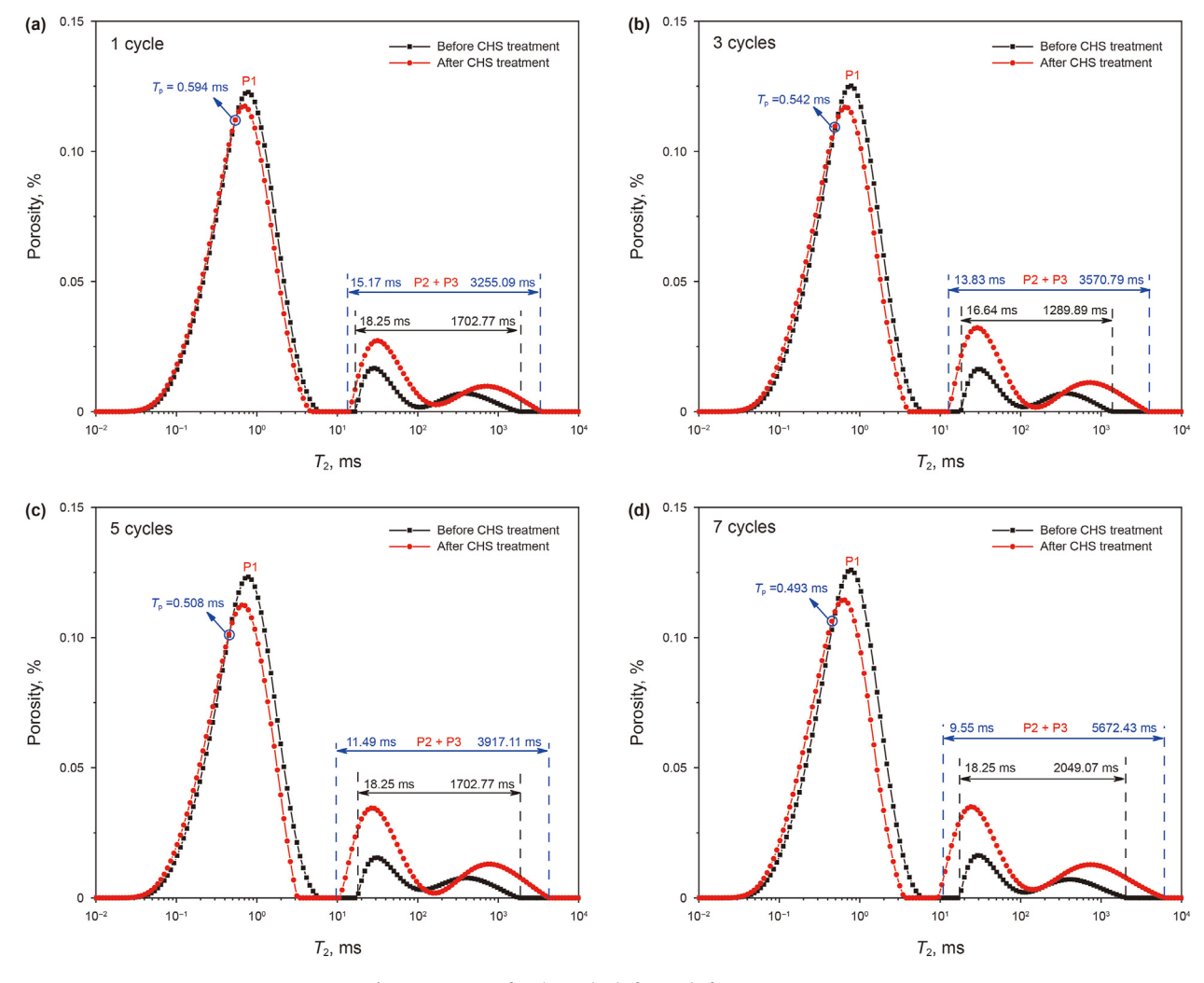


Fig. 2.  $T_2$  spectra of coal samples before and after CHS treatment.

R.-S. Ma, J.-Y. Zhang, Q.-H. Feng et al. Petroleum Science 21 (2024) 3271–3287

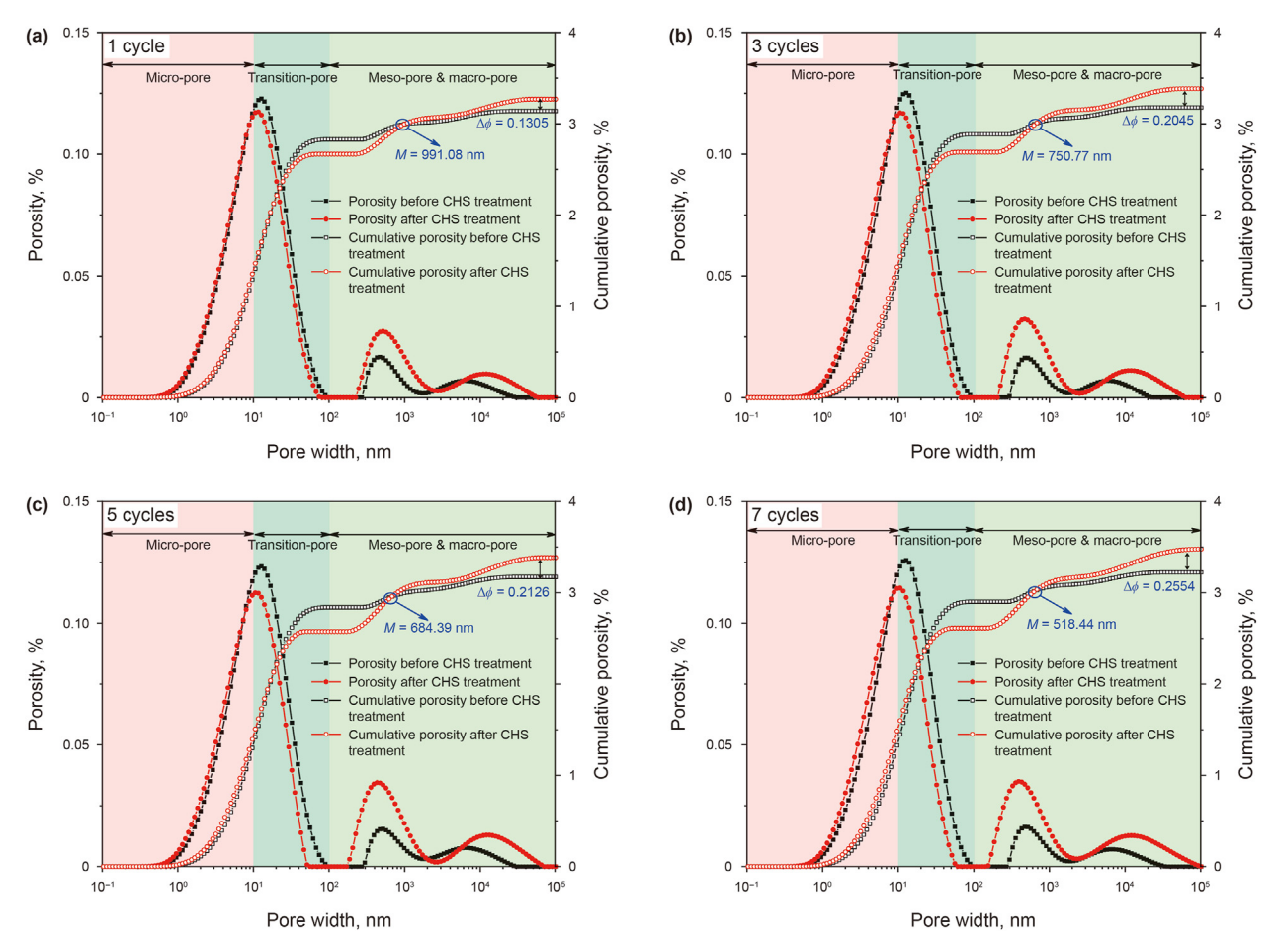


Fig. 3. PSD curves of coal samples before and after CHS treatment.

facilitates the generation and expansion of meso- and macro-pores. Nevertheless, after CHS treatment, the PSD curves of transition-pores collectively shift downward, indicating that the generation and expansion of meso- and macro-pores may compress the transition-pores. The PSD curves of micro-pores exhibit a more complex variation pattern, after CHS treatment, the PSD curves of micro-pores with smaller pore size exhibit an upward trend, while those of micro-pores with larger pore size display a downward trend. One reasonable explanation is that a portion of the micro-pores with larger pore size and the transition-pores were compressed into smaller-sized micro-pores.

Comparing the PSD curves of cumulative porosity before and after CHS treatment, it can be seen that there is an intersection point (M) between the CHS treated and untreated coal samples. When the pore size is smaller than M, the PSD curves of untreated coal samples are above those of CHS treated samples, indicating that the increase in porosity of meso- and macro-pores cannot offset the decrease in porosity of transition-pores. However, when the pore size is larger than M, the PSD curves of untreated samples are below those of CHS treated samples, suggesting that the increase in porosity of meso- and macro-pores plays a primary role in the change of cumulative porosity. It can also be found that after 1, 3, 5, and 7 hydraulic stimulation cycles, the value of *M* decreases to 991.08, 750.77, 684.39, and 518.44 nm, respectively. It means that as the number of hydraulic stimulation cycles increases, the effect of the decrease in porosity of transition-pores on cumulative porosity gradually diminishes. In addition, the overall porosity of the coal samples treated with CHS are significantly greater than that of the

untreated coal samples. It means that the impact of CHS on mesoand macro-pores is more pronounced than that on micro-pores and transition-pores. After 1, 3, 5, and 7 hydraulic stimulation cycles, the overall porosity increased by 0.1305%, 0.2045%, 0.2126%, and 0.2554%, respectively, indicating that a greater number of hydraulic stimulation cycles corresponds to stronger generation and expansion effects of meso- and macro-pores.

To quantitatively analyze the impact of hydraulic stimulation cycles on porosity, cumulative porosity for different pore types are extracted. Subsequently, the increment of cumulative porosity for each pore type is defined and calculated.

$$\Delta \phi = \phi_{i} - \phi_{0} \tag{3}$$

where  $\phi_i$  is the cumulative porosity after CHS treatment, %;  $\phi_0$  is the cumulative porosity before CHS treatment, %.

From Fig. 4, it can be found that the increment of porosity  $(\Delta\phi)$  of micro-pores, meso-pores, and macro-pores increases with the number of hydraulic stimulation cycles, whereas the  $\Delta\phi$  of transition pores exhibits an opposite trend compared to the other pore types. Additionally, an initial rapid increase is observed in the  $\Delta\phi$  of micro-pores, meso-pores, and macro-pores. Meanwhile, the  $\Delta\phi$  of transition-pores experiences a rapid decrease in the initial stage, which is followed by a gradual deceleration in the rate of decrease. It means that the initial hydraulic stimulation has a significant impact on porosity changes, whereas the effect of CHS on porosity changes gradually weakens as the number of hydraulic stimulation cycles increases. One potential explanation is that there is a

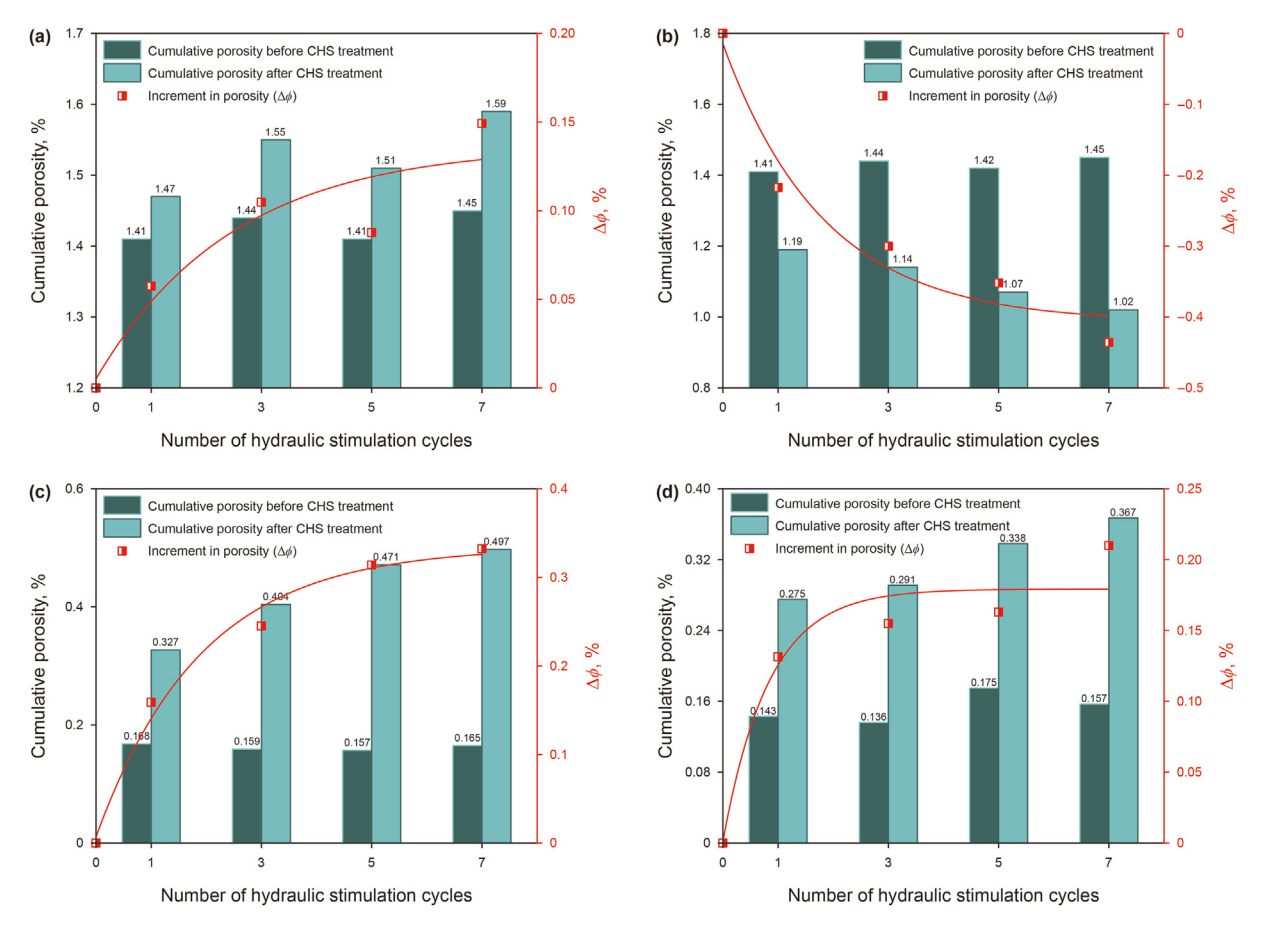


Fig. 4. Changes in cumulative porosity for different pore types before and after CHS treatment. (a) Micro-pores; (b) Transition-pores; (c) Meso-pores; (d) Macro-pores.

significant number of different types of pores before CHS treatment, leading to the porosity susceptible to the impact of the initial hydraulic stimulation. However, as the number of hydraulic stimulation cycles increases, the number of pores susceptible to hydraulic stimulation gradually decreases, ultimately resulting in limited changes in porosity.

## 3.1.3. Fractal characteristics based on NMR

The fractal dimensions are widely used to characterize surface roughness and the complexities of pore structures in coal. The calculation method of NMR fractal dimensions is as follows (Zhang et al., 2022):

$$lg(\varepsilon) = (3 - D_N)lg(T_2) + (D_N - 3)lg(T_{2max})$$
 (4)

where  $\varepsilon$  is the cumulative porosity with transverse relaxation time less than  $T_2$ , %;  $T_{2\text{max}}$  is the maximum transverse relaxation time, ms;  $D_N$  is the fractal dimension.

Previous studies have demonstrated that the sorption space for methane is mainly composed of micro- and transition-pores (< 100 nm), whereas meso- and macro-pores (> 100 nm) control the flow behavior of fluid (Liu et al., 2021). Therefore, taking  $T_2$  value corresponding to 100 nm as the dividing point, the curve with  $\lg(\varepsilon)$  as the vertical coordinate and  $\lg(T_2)$  as the horizontal coordinate can be divided into two parts. The surface fractal dimension ( $D_{N1}$ ) and the volume fractal dimension ( $D_{N2}$ ) can be obtained by linear fitting of the respective curve segments, as shown in Fig. 5.  $D_{N1}$  reflects the roughness and heterogeneity of sorption pore surface, and  $D_{N2}$  characterizes the complexity and connectivity of seepage pores (Shao et al., 2017). As can be seen from Fig. 5, the fitting

correlation coefficients of seepage pores (0.9035–0.9723) are greater than those of sorption pores (0.8313–0.8727), indicating that the seepage pores exhibit more evident fractal properties than the sorption pores. In addition, it can also be found from Fig. 5 that the values of  $D_{\rm N2}$  (2.9546–2.9779) are greater than those of  $D_{\rm N1}$  (2.0753–2.1529). It means that the seepage pores reveal a stronger complexity than that of sorption pores.

To quantitatively analyze the impact of hydraulic stimulation cycles on the fractal dimensions obtained from NMR, the increment of fractal dimension was defined and calculated.

$$\Delta D_{Ni} = D_{Ni} - D_{N0} \tag{5}$$

where  $D_{\mathrm{N}i}$  is the fractal dimensions after CHS treatment;  $D_{\mathrm{N}0}$  is the fractal dimensions before CHS treatment; i=1 represents the surface fractal dimension; i=2 represents the volume fractal dimension.

Fig. 6 illustrates that the  $D_{\rm N1}$  of the samples treated with CHS are less than those of the untreated samples, whereas the  $D_{\rm N2}$  of the samples show an opposite trend. The increase in  $D_{\rm N1}$  indicates an increase in the roughness of the sorption pore surface after CHS treatment. The decrease in  $D_{\rm N2}$  implies that the heterogeneity of seepage pores was decreased after CHS treatment. In addition, as can be seen from Fig. 6, with the increase in the number of hydraulic stimulation cycles,  $\Delta D_{\rm N1}$  increases rapidly in the initial stage, and then the growth rate gradually decreases, while the trend of  $\Delta D_{\rm N2}$  is opposite to that of  $\Delta D_{\rm N1}$ . It means that the initial hydraulic stimulation plays a significant role in the change of fractal dimensions, which is consistent with the trend of porosity.

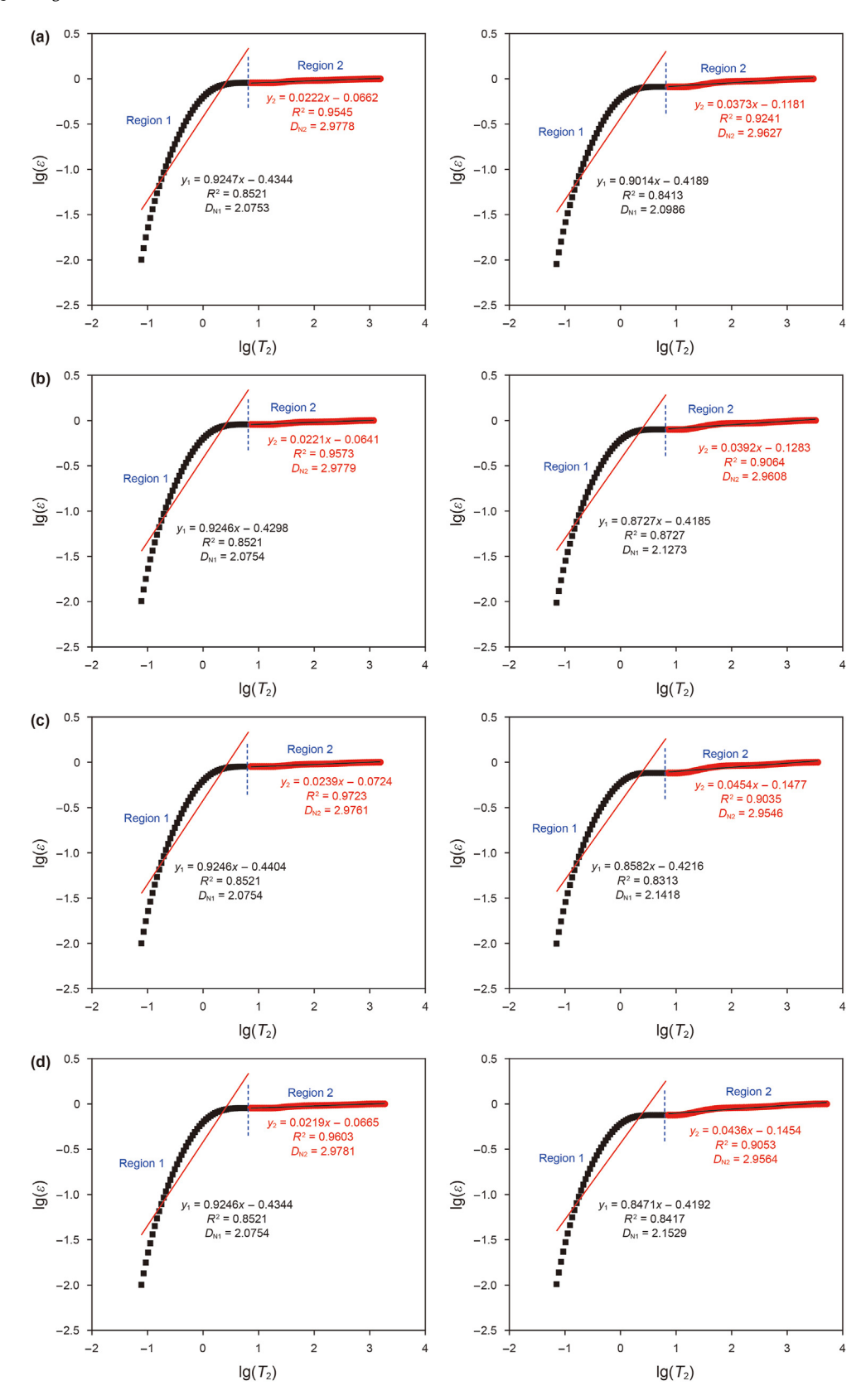


Fig. 5. Plots of  $\lg(e)$  vs.  $\lg(T_2)$  from NMR testing data of samples before (left) and after (right) CHS treatment with 1 (a), 3 (b), 5 (c), and 7 (d) cycles, respectively.

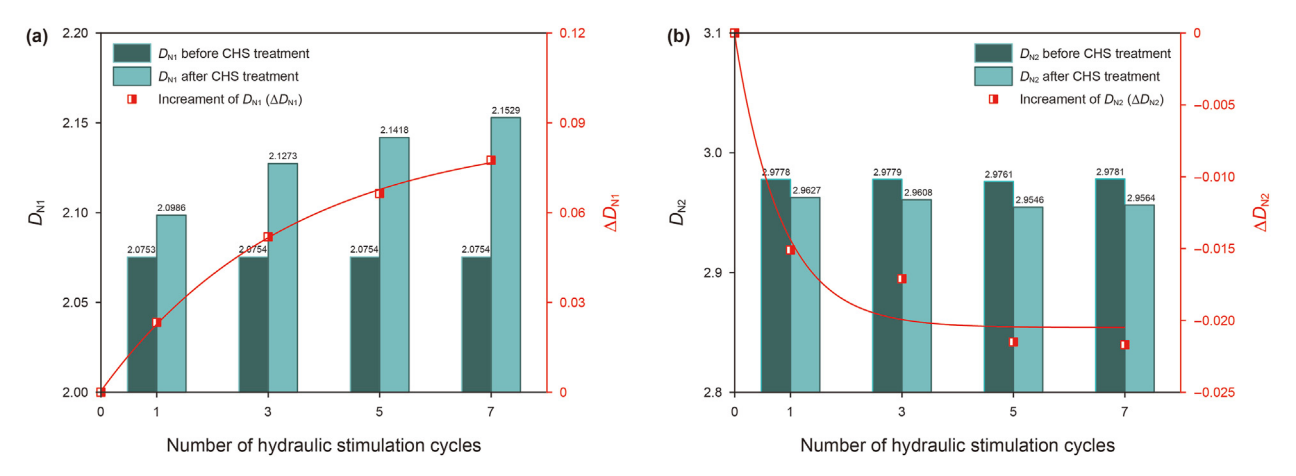


Fig. 6. Changes in fractal dimensions before and after CHS treatment obtained from NMR. (a) The surface fractal dimension; (b) The volume fractal dimension.

# 3.2. LTNS analysis

# 3.2.1. Low temperature nitrogen sorption-desorption curves

In Fig. 7, the nitrogen sorption process can be categorized into three stages. At low relative pressure ( $0 < P/P_0 < 0.1$ ), nitrogen

undergoes monolayer sorption on the pore surface, resulting in a rapid increase in the sorption isotherm within a short period. When the relative pressure increases from 0.1 to 0.5, the sorption isotherm increases slowly at a relatively constant rate, indicating that the sorption form of nitrogen on the pore surface transitions

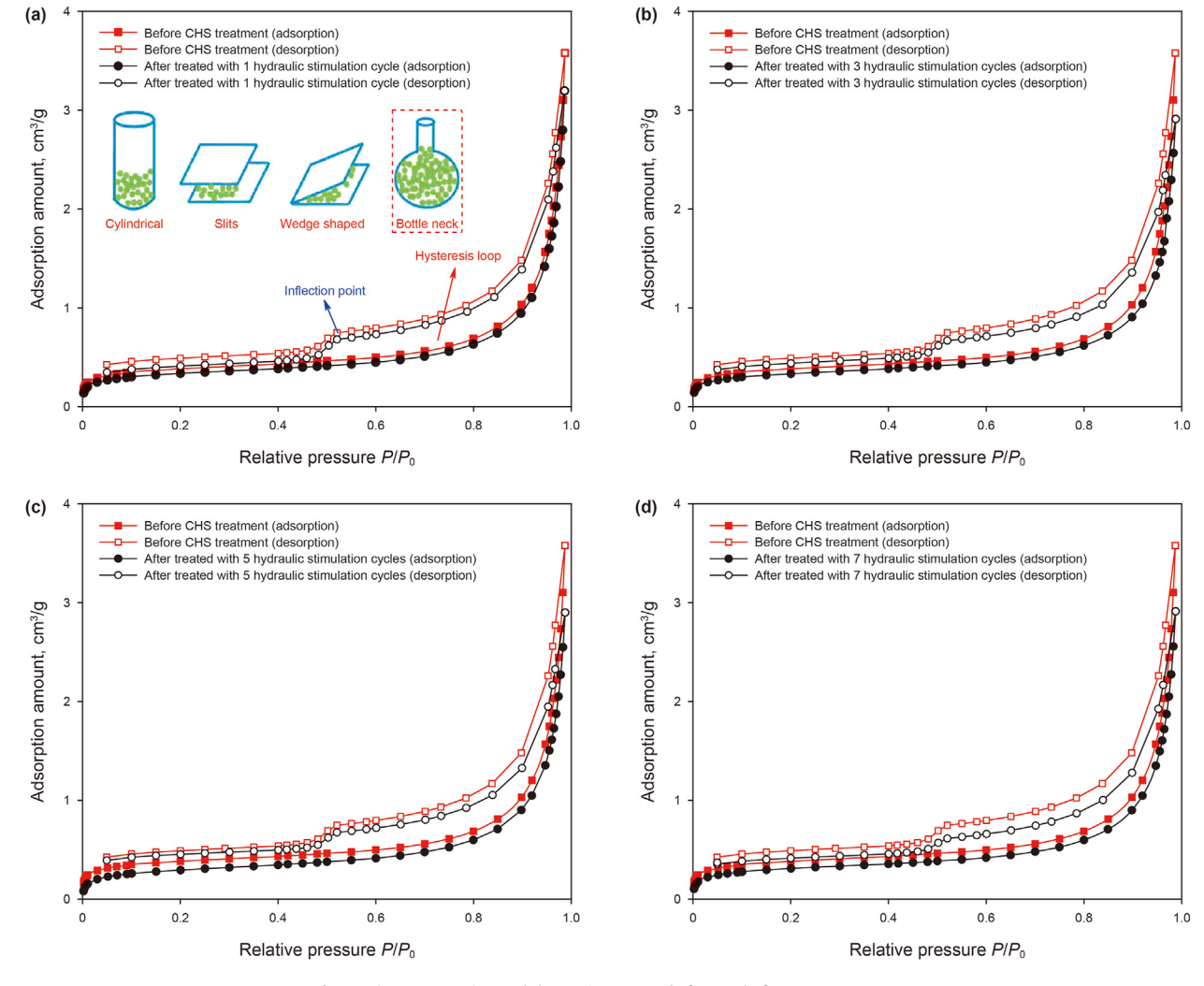


Fig. 7. Nitrogen sorption and desorption curves before and after CHS treatment.

from monolayer to multilayer. As the relative pressure is greater than 0.5, nitrogen sorption amount increases rapidly due to capillary condensation in the pores. However, it is noteworthy that as the relative pressure approaches 1, nitrogen fails to reach sorption saturation. This is primarily attributed to the presence of a significant number of pores with sizes exceeding 300 nm in the coal samples, making it challenging for nitrogen to attain sorption saturation in these pores (Clarkson et al., 2013).

It should be noted that, as the relative pressure decreases, the condensed nitrogen in the pores gradually undergoes evaporation and desorption. If the relative pressures for condensation and evaporation are equal, the sorption isotherm and desorption isotherm coincide. When the two relative pressures are different, a hysteresis loop is formed (Xue et al., 2021). In addition, previous studies have shown that there is a significant correlation between the shape of hysteresis loops and pore morphology. Specifically, based on the shape of hysteresis loops, coal pores can be classified into four different types (Fig. 7(a)) (Sing, 1985). Different pore types are associated with different desorption isotherms, resulting in different shapes of hysteresis loops. Notably, for ink-bottle-shaped pores, due to the existence of a thin neck structure, the desorption isotherm consistently exhibits a sharp decrease at the inflection point (Fu et al., 2017). As illustrated in Fig. 7, the sorption and desorption isotherms of all tested coal samples do not coincidence, and near the inflection point ( $P/P_0 = 0.5$ ), the desorption isotherms exhibit a sharp drop. The results suggest that the pore morphology of the tested coal samples is dominated by ink bottle-shaped pores. Furthermore, there is little difference in the shape of the hysteresis loops before and after CHS treatment. It means that the main pore morphology in coal samples has not changed after CHS treatment.

# 3.2.2. Analysis of pore structure parameters based on LTNS

To elucidate the changes in pore structure parameters of various pore types before and after CHS treatment, the data of specific surface area and pore volume were extracted separately. The increments of specific surface area ( $\Delta S$ ) and pore volume ( $\Delta V$ ) of different pore types were defined and calculated.  $\Delta S$  and  $\Delta V$  were calculated as follows:

$$\Delta S = S - S_0 \tag{6}$$

$$\Delta V = V - V_0 \tag{7}$$

where  $S_0$  and S are the specific surface area of coal samples before and after CHS treatment, cm<sup>2</sup>/g;  $V_0$  and V are the pore volume of coal samples before and after CHS treatment, cm<sup>3</sup>/g.

Figs. 8 and 9 illustrate the changes in pore structure parameters before and after CHS treatment obtained from the LTNS test. However, due to the limitation of LTNS testing (< 300 nm) (Su et al., 2021), the pore structure parameters for macro-pores cannot be provided. In Fig. 8, the pore volume of transition-pores ( $V_{\text{tran}}$ ) of the untreated coal sample is  $4.52 \times 10^{-3}$  cm<sup>3</sup>/g, whereas the  $V_{\text{tran}}$  of coal samples treated with 1, 3, 5, and 7 hydraulic stimulation cycles decreases to  $2.94 \times 10^{-3}$ ,  $2.62 \times 10^{-3}$ ,  $2.30 \times 10^{-3}$ , and  $1.98 \times 10^{-3}$  cm<sup>3</sup>/g, respectively. However, with the increase in hydraulic stimulation cycles, the pore volume of micro-pores ( $V_{\rm mic}$ ) and meso-pores ( $V_{\text{meso}}$ ) exhibit an opposite trend compared to  $V_{\text{tran}}$ . The results are consistent with the variation trend of each pore type obtained from NMR, further confirming the hypothesis that CHS promotes the expansion and generation of meso- and macro-pores, and compress a portion of larger-sized micro- and transition-pores into smaller-sized micro-pores. Additionally, it should be noted that the total pore volume  $(V_t)$  of the untreated coal sample is  $7.33 \times 10^{-3}$  cm<sup>3</sup>/g. After the samples treated with 1, 3, 5, and 7 hydraulic stimulation cycles, the  $V_t$  decreases to

 $6.61 \times 10^{-3}$ ,  $6.08 \times 10^{-3}$ ,  $5.87 \times 10^{-3}$ , and  $5.85 \times 10^{-3}$  cm<sup>3</sup>/g, respectively. The result indicates that an increase in the number of hydraulic stimulation cycles leads to a reduction in  $V_t$ , which is opposite to the NMR result.

Fig. 9 illustrates that after the coal samples treated with 1, 3, 5 and 7 hydraulic stimulation cycles, the total specific surface area  $(S_t)$  decreased from 0.636 to 0.538, 0.516, 0.505, and 0.491 m<sup>2</sup>/g, respectively. The result indicates that the S<sub>t</sub> of coal sample decreases with increasing hydraulic stimulation treatment cycles, and the initial hydraulic stimulation has the most significant impact on the increment of total specific surface area ( $\Delta S_t$ ), which is consistent with the variation trend of total pore volume but opposite to the trend of total pore porosity. After CHS treatment, the specific surface area of different pore types exhibits different trends, both the specific surface area of micro-pores  $(S_{mic})$  and meso-pores  $(S_{meso})$ increase with the increase in the number of hydraulic stimulation cycles, while the specific surface area of transition-pores ( $S_{tran}$ ) shows a downward trend, which is consistent with the variation trend of pore volume and the trend of pore porosity. In addition, the values of  $S_{mic}$  and  $S_{tran}$  are one order of magnitude greater than the value of S<sub>meso</sub>, indicating that the total specific surface area of coal is contributed by micro- and transition-pores, which is consistent with previous findings.

### 3.2.3. Fractal characteristics based on LTNS

Up to now, various methods have been proposed for calculating the fractal dimension based on nitrogen sorption isotherms, with the Frenkel—Halsey—Hill (FHH) model considered to be the most effective (Pyun et al., 2004). In the FHH model, fractal dimension is generally between 2 and 3 (Pfeifer et al., 1989). When the fractal dimension is 2, it represents a perfectly smooth pore surface and an extremely simple pore structure. Conversely, a fractal dimension of 3 indicates that the pore surface is completely irregular or rough, and the pore structure is highly heterogeneous. According to nitrogen sorption data and the FHH model, the fractal dimension can be determined by the following equations (Wang and Guo, 2021; Yang et al., 2023):

$$ln(V/V_0) = A ln[ln(P_0/P)] + B$$
 (8)

where P is the nitrogen sorption equilibrium pressure, MPa;  $P_0$  is the saturation vapor pressure, MPa; V is the sorption amount of nitrogen at the equilibrium pressure P,  $cm^3/g$ ;  $V_0$  is the sorption amount of nitrogen at the saturation vapor pressure  $P_0$ ,  $cm^3/g$ ; A is the linear correlation coefficient; B is a constant. The relationship between A and fractal dimension ( $D_L$ ) can be expressed as

$$D_{L} = A + 3 \tag{9}$$

The alterations in nitrogen sorption isotherms are related to two mechanisms: (1) When the relative pressure is less than 0.5, the adsorption of nitrogen on the coal surface is mainly controlled by van der Waals forces between nitrogen molecules and coal molecules (Yao et al., 2008). (2) When the relative pressure is greater than 0.5, the increase in sorption amount is primarily attributed to the capillary condensation of nitrogen molecules within the pores (Yin et al., 2018). Therefore, bounded by the relative pressure of 0.5, nitrogen sorption data can be divided into two parts, and then the fractal dimension  $D_{L1}$  ( $P/P_0 < 0.5$ ) and  $D_{L2}$  ( $P/P_0 > 0.5$ ) can be obtained. DL1 is linked to pore surface morphology, serving as an indicator of pore surface roughness (Yuan and Rezaee, 2019). DL2 is associated with the pore structure, providing a measure of the irregularity of seepage pores (Brunauer et al., 1938). By combining the FHH model with nitrogen sorption data, a linear relationship between  $ln(V/V_0)$  and  $ln[ln(P/P_0)]$  was established, from which the

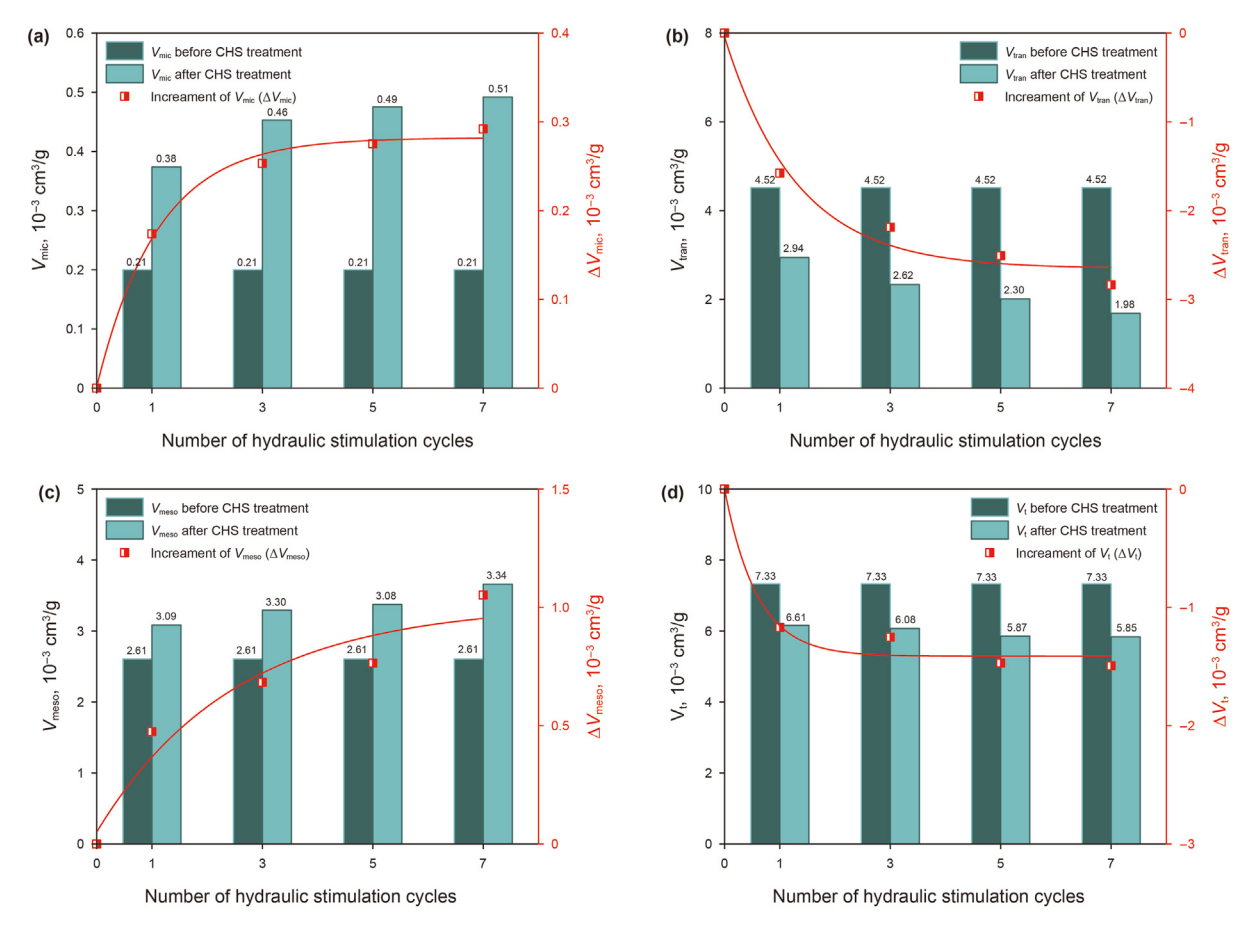


Fig. 8. Changes in pore volume of different pore types of coal samples before and after CHS treatment. (a) Micro-pores; (b) Transition-pores; (c) Meso-pores; (d) Total pores.

fractal dimension  $D_L$  was calculated (Fig. 10).

As can be seen from Fig. 10, all correlation coefficients ( $R^2$ ) are greater than 0.9, indicating that the pore surface morphology and pore structure of coal samples both exhibit strong fractal characteristics. In addition, it also can be found that the correlation coefficients of region 1 (0.9136-0.9364) is less than that of region 2 (0.9939-0.9981). It means that the fractal characteristics of pore surface morphology is stronger than that of pore structure. Furthermore, it is noteworthy that the value ranges of  $D_{11}$  and  $D_{12}$ are 2.5572–2.5923 and 2.4663–2.4943, respectively ( $D_{L1} > D_{L2}$ ). The result suggests that the heterogeneity of pore surface morphology is more pronounced than that of pore structure. To quantitatively assess the impact of the number of hydraulic stimulation cycles on the fractal dimension obtained from LTNS, the incremental change in fractal dimension was calculated by Eq. (5). Fig. 11 illustrates that, as the number of hydraulic stimulation cycles increases,  $\Delta D_{\rm L1}$  demonstrates an upward trend, while  $\Delta D_{\rm L2}$  exhibits a downward trend. It means that after CHS treatment, there was an increase in the roughness of the pore surface and a decrease in the complexity of seepage pores. This finding is consistent with the result of fractal dimensions obtained from NMR.

#### 3.3. Methane sorption characteristics

# 3.3.1. Methane sorption isothermal

The experimental results of methane isothermal sorption for all tested coal samples are presented in Fig. 12, where the effectiveness of the Langmuir model in describing the methane sorption processes is evident. Moreover, it can also be found that, at the same

equilibrium pressure, the methane sorption amount of coal samples treated with CHS is generally lower than that of untreated samples. As the hydraulic stimulation cycle increases, the methane sorption isotherm generally shows a trend of rapid decrease at first and then the decline rate gradually slowed down.

To quantitatively analyze the impact of CHS on coal sorption characteristics, the Langmuir volume and Langmuir pressure were extracted. Subsequently, the increments of Langmuir volume and Langmuir pressure were defined and calculated as follows:

$$\Delta V_{\rm L} = V_{\rm L} - V_{\rm L0} \tag{10}$$

$$\Delta P_{\rm L} = P_{\rm L} - P_{\rm L0} \tag{11}$$

where  $V_{L0}$  and  $V_L$  is the Langmuir volume before and after CHS treatment, cm<sup>3</sup>/g;  $P_{L0}$  and  $P_L$  is the Langmuir pressure before and after CHS treatment, MPa.

As can be seen from Fig. 13, the Langmuir volume and Langmuir pressure of samples untreated with CHS are 33.47 cm³/g and 0.256 MPa, respectively. After the samples treated with 1, 3, 5, and 7 hydraulic stimulation cycles, the Langmuir volume decreased to 28.05, 25.71, 25.51, and 24.18 cm³/g, respectively. The corresponding Langmuir pressure decreased to 0.205, 0.193, 0.186, and 0.176 MPa, respectively. The results indicate that with an increase in the number of hydraulic stimulation cycles, the maximum sorption amount of coal for methane gradually decreases. Furthermore, under a given pressure drop for initial gas depletion, the desorption rate of methane from the coal samples treated with CHS is less than that from the untreated samples. It can also be found that the

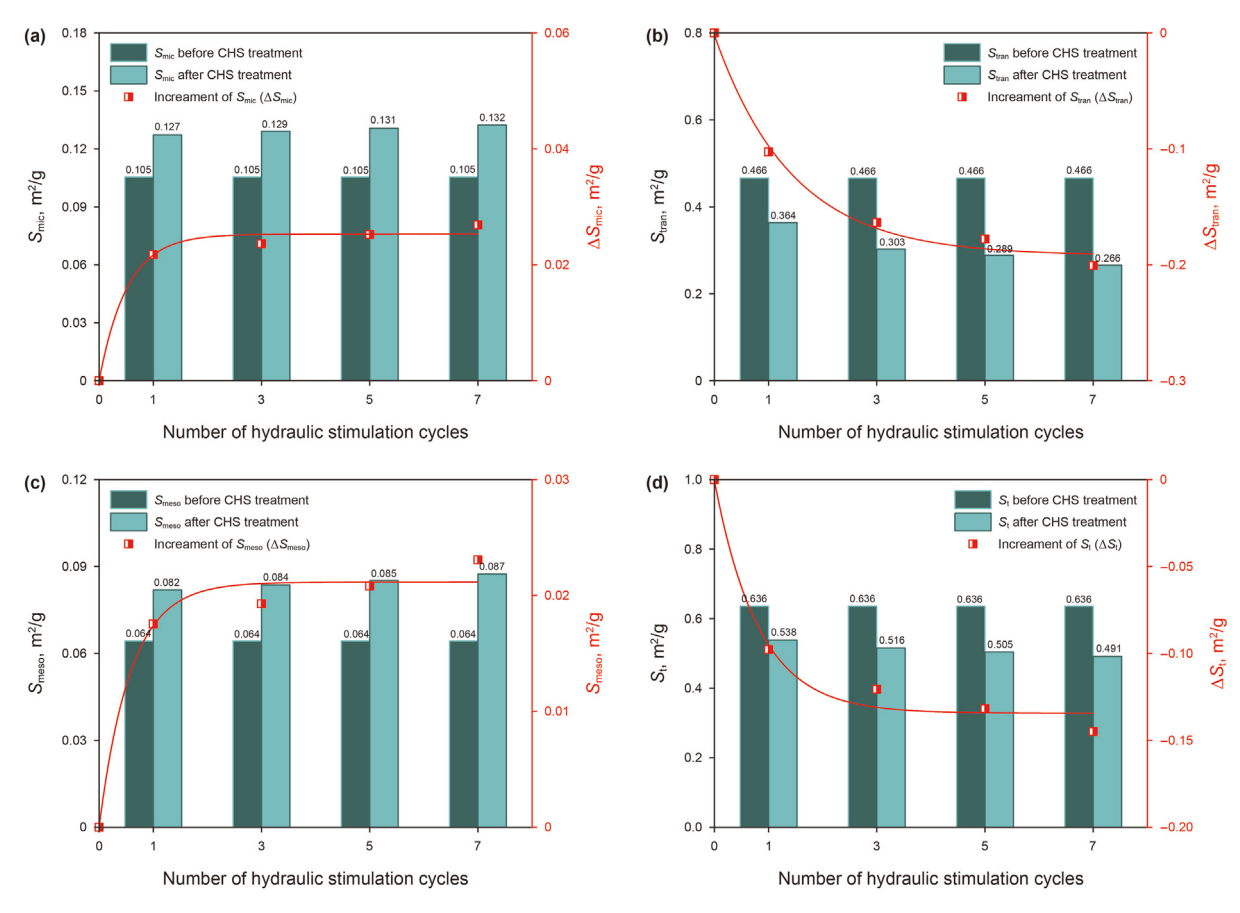
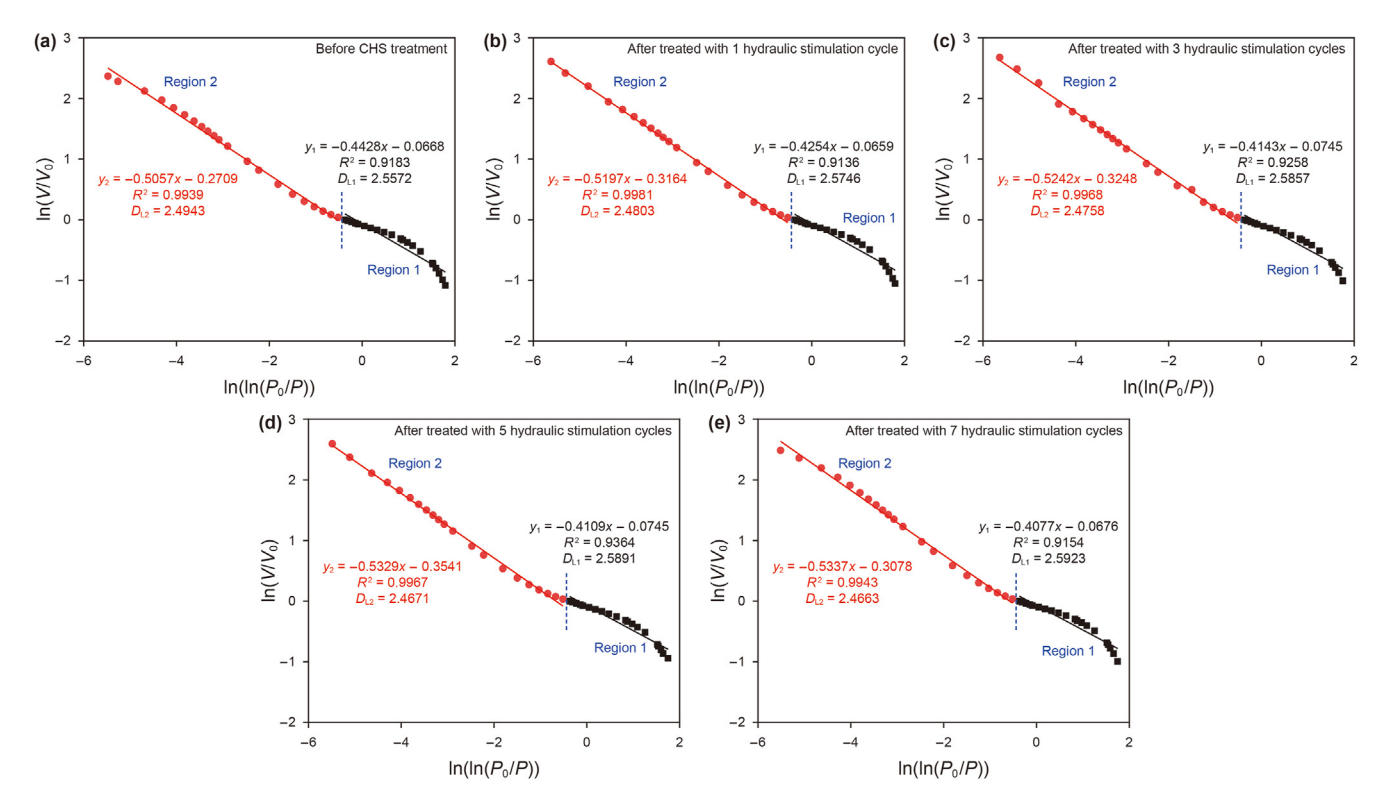


Fig. 9. Changes in specific surface area of different pore types of coal samples before and after CHS treatment. (a) Micro-pores; (b) Transition-pores; (c) Meso-pores; (d) Total pores.



**Fig. 10.** A linear relationship between  $\ln(V/V_0)$  and  $\ln(\ln(P_0/P))$  from LTNS testing data.

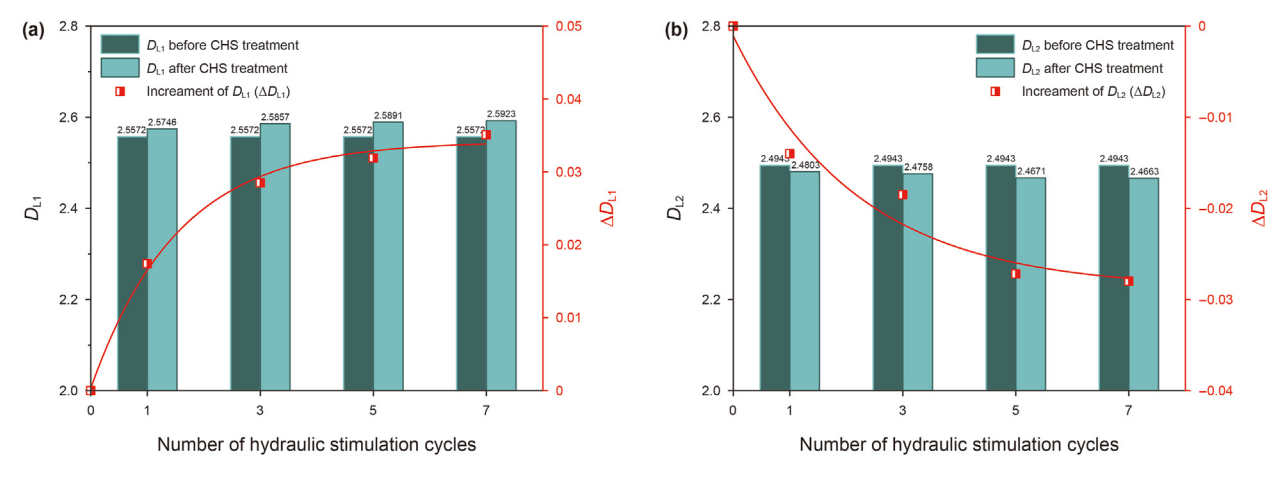


Fig. 11. Changes in fractal dimensions of coal samples before and after CHS treatment obtained from LTNS.

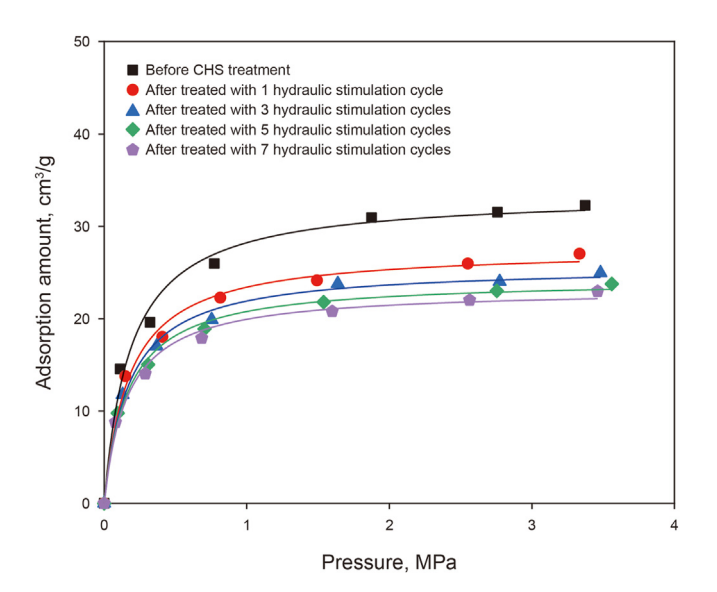
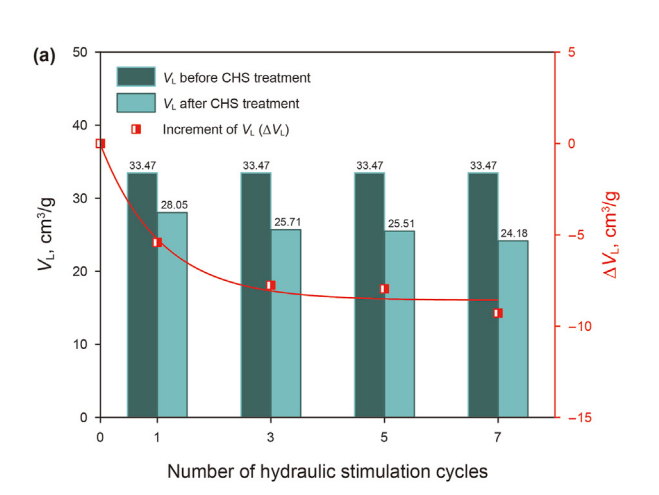


Fig. 12. Methane isothermal sorption curves of coal samples before and after CHS treatment.

decrease in the increments of Langmuir volume and Langmuir pressure is primarily attributed to the impact of initial hydraulic stimulation.



3.3.2. Relationship between methane sorption characteristics and pore structure parameters

Fig. 14 illustrates the correlation between methane sorption characteristics and pore structure parameters,  $\Delta V_{\rm L}$  and  $\Delta P_{\rm L}$  exhibit a positive correlation with  $\Delta S_t$  and  $\Delta V_t$ , while showing a negative correlation with the increment of total porosity ( $\Delta \phi_t$ ). The methane sorption characteristic parameters ( $\Delta V_{\rm I}$ ,  $\Delta P_{\rm I}$ ) present a stronger correlation with  $\Delta S_t$  than with  $\Delta V_t$  and  $\Delta \phi_t$ . The results indicate that the methane sorption characteristics of coal are primarily associated with the surface area, which is consistent with previous studies. Moreover, the correlation coefficients between  $\Delta V_t$  and  $\Delta V_{\rm I}$ ,  $\Delta P_{\rm I}$  are 0.92 and 0.93, respectively, which are larger than those between  $\Delta \phi_t$  and  $\Delta V_L$   $\Delta P_L$ . It means that the changes in methane sorption characteristics presents a stronger correlation with  $\Delta V_t$ than with  $\Delta \phi_t$ . The differences in the correlation between methane adsorption characteristics and the increment of total pore volume may be attributed to the larger sample size used in the NMR, which provides more comprehensive information about pore and fracture structures compared to the LTNS. However, the impact of this additional information on pore structure parameters is primarily reflected in pore volume rather than specific surface area.

# 3.3.3. Relationship between methane sorption characteristics and surface fractal dimensions

To further clarify the relationship between methane sorption characteristics and surface fractal dimension, combined with NMR, LTNS and methane isothermal sorption analysis, the relationship

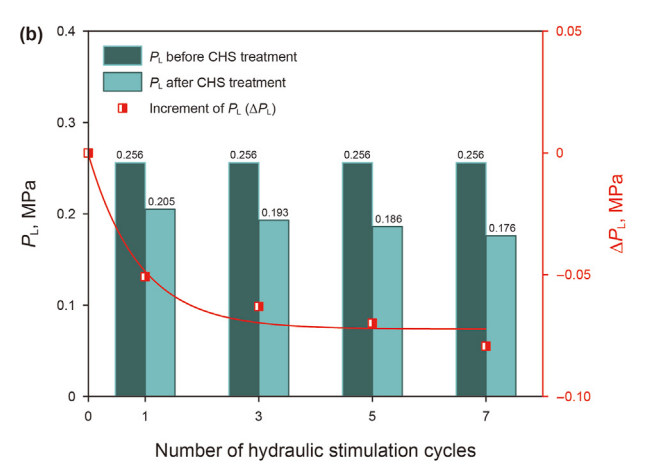


Fig. 13. Changes in Langmuir volume and Langmuir pressure before and after CHS treatment.

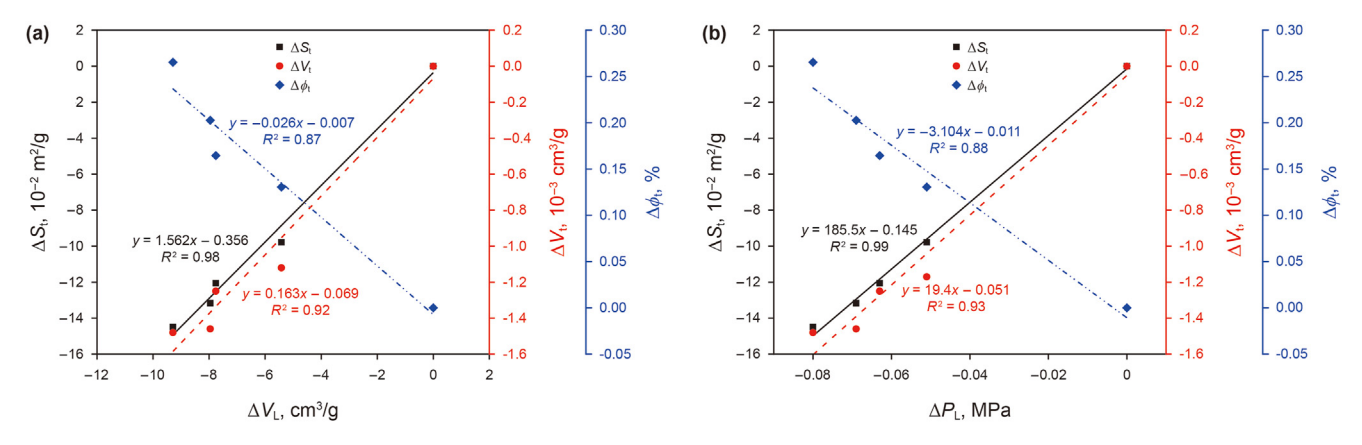


Fig. 14. Relationship between increments of Langmuir volume and Langmuir pressure  $(\Delta V_L, \Delta P_L)$  and pore structure parameters.

between increments of Langmuir volume and Langmuir pressure  $(\Delta V_{\rm I}, \Delta P_{\rm I})$  and surface fractal dimensions  $(\Delta D_{\rm II}, \Delta D_{\rm NI})$  for the tested samples were obtained. As shown in Fig. 15, there is a strong negative correlation between  $\Delta V_{\rm L}$ ,  $\Delta P_{\rm L}$  and  $\Delta D_{\rm L1}$ ,  $\Delta D_{\rm N1}$ , indicating that the surface fractal dimensions can be used as an important parameter reflecting the methane sorption capacity of coal. It should be noted that the correlation coefficients between  $\Delta V_{\rm I}$ ,  $\Delta P_{\rm I}$ and  $\Delta D_{\rm I,1}$  are greater than those between  $\Delta V_{\rm L}$ ,  $\Delta P_{\rm L}$  and  $\Delta D_{\rm N1}$ . It means that  $\Delta D_{1,1}$  serves as a more effective parameter than  $\Delta D_{N,1}$  in reflecting the changes in coal sorption characteristics for methane, indicating that  $\Delta D_{1,1}$  reflects more comprehensive information about pore surface than  $\Delta D_{\rm N1}$ . This is primarily attributed to the fact that  $D_{\rm N1}$  obtained from NMR is unable to capture the pore surface information for pores larger than 100 nm. In contrast, D<sub>L1</sub> obtained from LTNS provides a broader range of pore surface information (< 300 nm).

# 4. Discussion

# 4.1. Effect of CHS on pore structure parameters

Both the results of NMR and LTNS show that after CHS treatment, meso- and macro-pores tend to be enlarged and generated, whereas micro-pores with larger sizes and transition-pores may be compressed into smaller-sized micro-pores. However, it should be noted that NMR result indicates an increase in cumulative porosity with an increase in the number of hydraulic stimulation cycles,

contrary to the LTNS result. This contradiction may be attributed to the limitation of LTNS, which is only suitable for pores with diameters smaller than 300 nm (Ozdemir, 2016). Additionally, from the NMR results (Fig. 3), it can be observed that when the pore width is less than 300 nm, the cumulative porosity of the coal sample after CHS treatment is lower than that before CHS treatment, which is consistent with the decrease in total pore volume obtained from LTNS. Thus, we can infer that when the pore width is less than 300 nm, the expansion of meso- and macro-pores cannot fully compensate for the decrease in pore volume caused by pore compression, resulting in a decrease in the total pore volume obtained from LTNS.

Fig. 9 presents that the  $S_{\rm mic}$  and  $S_{\rm meso}$  increase with the increase in the number of hydraulic stimulation cycles, while the  $S_{\rm tran}$  shows a downward trend, which is consistent with the variation trend of pore volume and the trend of pore porosity. The variation mechanisms of  $S_{\rm meso}$  may be attributed to the following two reasons: (1) Due to the enlargement of meso-pores, part of smaller meso-pores is transformed into larger ones. (2) Due to the generation of meso-pores, the number of meso-pores are increased. The variation mechanism of  $S_{\rm mic}$  and  $S_{\rm tran}$  is mainly due to the compression of micro-pores with larger sizes and transition-pores into smaller-sized micro-pores. Specifically, after CHS treatment, there is a decrease in the number of transition pores and an increase in the number of micro-pores, resulting in a decrease in  $S_{\rm tran}$  but an increase in  $S_{\rm mic}$ . Comparing the sorption curves of coal samples for nitrogen before and after CHS treatment (Fig. 7), it can be observed

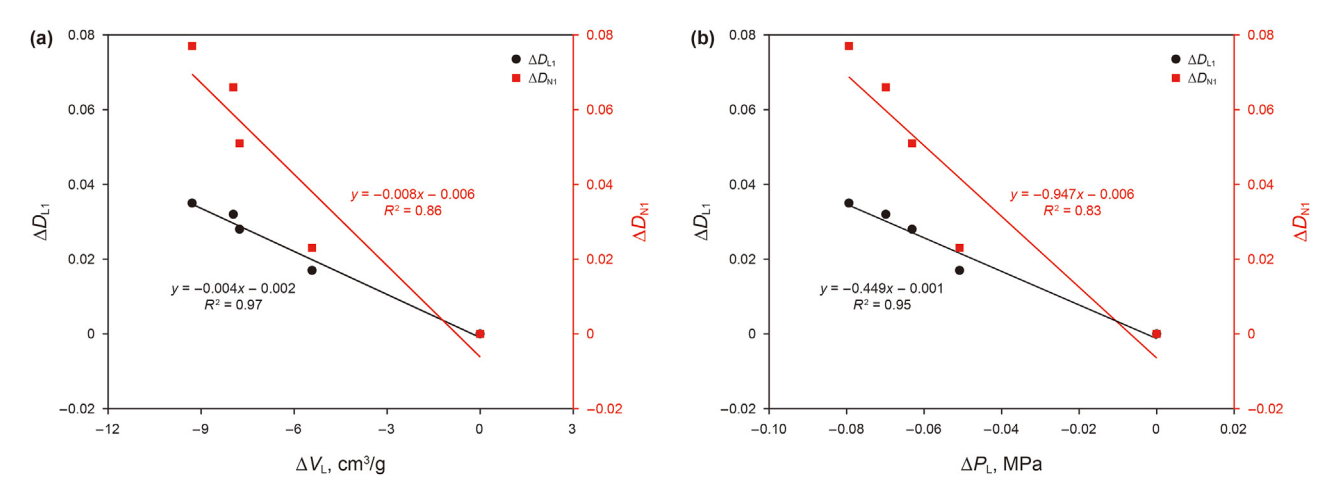


Fig. 15. Relationship between increments of Langmuir volume and Langmuir pressure  $(\Delta V_L, \Delta P_L)$  and surface fractal dimensions  $(\Delta D_{L1}, \Delta D_{N1})$ .

that the sorption curve of CHS treated samples are lower than of untreated sample. It mainly attributed to the fact that the mic- and transition-pores provide the majority of specific surface area of coal (Chen et al., 2017), the increase in specific surface area resulting from the expansion and generation of meso- and micro-pores cannot fully compensate for the decrease in specific surface area due to the compression of micro-pores with larger sizes and transition-pores, resulting in a decrease in total specific surface area.

# 4.2. Effect of CHS on fractal characteristics

For coal, there are relatively smooth regions and rough regions on the pore wall surface, and the values of surface fractal dimensions  $(D_{N1}, D_{L1})$  are determined by the proportion of rough regions of pore surface (Xue et al., 2021). As previous mentioned, there is an increase in the surface fractal dimensions of coal after CHS treatment, indicating that the rough regions of pore surface of coal are increased after CHS treatment. This may be attributed to the compression effect of mic- and transition-pores, which leads to pore constriction and results in the overall surface of the sorption pores changing from relatively regular to irregular, as shown in Fig. 16(a) and (b). For the decrease in volume fractal dimension  $(D_{N2}, D_{12})$ , one possible explanation is that the expansion and generation of meso- and macro-pores improved the connectivity of seepage pores, as shown in Fig. 16(c) and (d). This result is similar to the findings of Zhou et al. (2021), who observed a significant decrease in the heterogeneity of water distribution in flow channels after increasing hydraulic fracturing injection pressure.

In addition, it should be noted that the pore surface fractal dimensions obtained from LTNS (2.5572–2.5923) are greater than those obtained from NMR (2.0753–2.1529). Conversely, the pore volume fractal dimensions obtained from LTNS (2.4643–2.4943) are less than those obtained from NMR (2.9546–2.9779). The difference in fractal dimensions obtained from NMR and LTNS methods may be attributed to their distinct physical contexts. The fractal dimensions derived from LTNS rely on the pore surface area and pore volume, while those obtained from NMR depend on the distribution of pore sizes (Zhou et al., 2020). Due to the limitation of LTNS, the fractal dimension  $D_{L2}$  cannot effectively capture pore parameter information associated with pore sizes larger than 300 nm. In contrast, the NMR supplies a broader pore size

distribution than LTNS, revealing a more extensive range of seepage pores. Hence, the values of  $D_{\rm N2}$  are greater than those of  $D_{\rm L2}$ , indicating a more complex pore structure discerned from NMR. Simultaneously, the fractal dimension  $D_{\rm N1}$  obtained from the NMR fails to capture the pore surface information of pores with sizes larger than 100 nm. In contrast, the LTNS provides more comprehensive pore surface information (< 300 nm) than that obtained from NMR. As a result, the values of  $D_{\rm L1}$  are greater than those of  $D_{\rm N1}$ , reflecting a more irregular pore surface discerned from LTNS.

# 4.3. Effect of CHS on sorption characteristics of coal for methane

The results of methane sorption isothermal indicate that after CHS treatment, the maximum sorption amount of coal for methane tends to decrease. This result is somewhat expected, as the TSSA of coal show a decreasing trend after CHS treatment. Based on the basic physical adsorption theory of solid surfaces, the maximum adsorption capacity of a solid is necessarily positively correlated with surface sorption sites (Laxminarayana and Crosdale, 1999). The greater the TSSA, the more surface sorption sites there are, resulting in a higher maximum adsorption amount (Zhao et al., 2016). After CHS treatment, the compression of mic- and transition-pores leads to an overall decrease in TSSA, thereby reducing the surface sites for CBM adsorption. Thus, Langmuir volume for coal shows a decreasing trend after CHS treatment. The value of Langmuir pressure reflects the adsorption rate of coal for methane, which is determined by the adsorption potential between coal and methane, and a smaller Langmuir pressure corresponds to a larger adsorption potential (Li H. et al., 2018). Previous study has shown that the adsorption potential is associated with the roughness of pore surface (Yang et al., 2019). As shown in Fig. 17(a), when the pore surface is relatively smooth, the methane molecule interacts only with one pore wall, and the sorption potential is equal to the planar sorption potential (W). As the surface roughness of the pores increases, the methane molecule fully interacts with one pore wall and partially with another (Fig. 17(b)). At this point, the adsorption potential of the methane molecules ranges from W to 2W. With further increase in the surface roughness of the pores, the methane molecule fully interacts with both sides of the pore walls, and the adsorption potential of the methane molecules is twice that of the planar adsorption potential (Fig. 17(c)). Thus, a greater pore surface roughness corresponds to a larger adsorption potential of

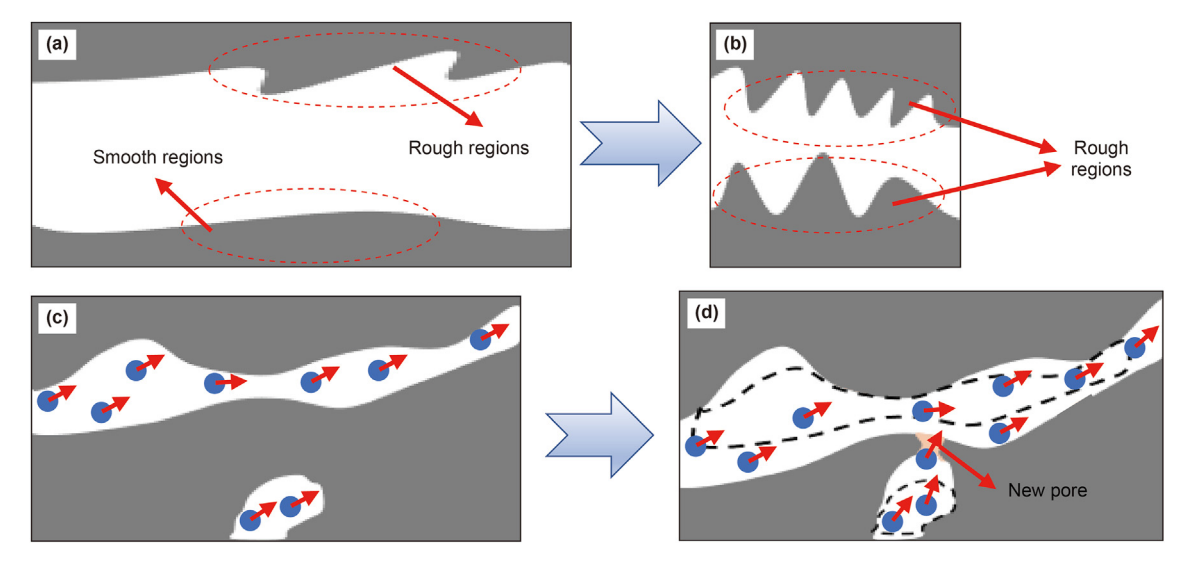
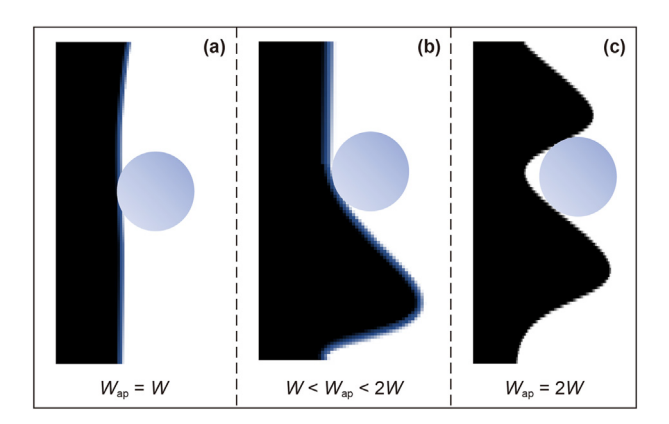


Fig. 16. Schematic of pore structure changes before and after CHS treatment.



**Fig. 17.** Schematic of relationship between pore surface roughness and adsorption potential. W and  $W_{\rm ap}$  represent the planar sorption potential and the actual adsorption potential of methane molecules, respectively.

coal. After CHS treatment, the compression of mic- and transitionpores leads to an increase in the overall pore surface roughness, thereby increasing the adsorption potential of coal for methane. Thus, Langmuir pressure for coal shows a decreasing trend after CHS treatment.

#### 5. Conclusions

The CHS technology holds promising applications in terms of environmental friendliness and permeability enhancement for CBM extraction. This study experimentally investigates the impact of CHS on the pore structure and methane sorption characteristics of anthracite from the Qinshui Basin. The following conclusions can be drawn.

- (1) CHS facilitates the generation and expansion of meso- and macro-pores, whereas micro-pores with larger sizes and transition-pores may be compressed into smaller-sized micro-pores. As the number of hydraulic stimulation cycles increases, the impact of pore compression on cumulative porosity gradually diminishes.
- (2) As micro- and transition-pores contribute majority of the specific surface area (SSA) in coal pores, the increase in SSA due to the expansion and generation of meso- and macropores fails to compensate for the decrease in SSA caused by the compression of transition-pores. After the coal samples treated with 1, 3, 5, and 7 hydraulic stimulation cycles, the total specific surface area (TSSA) decreased from 0.636 to 0.538, 0.516, 0.505, and 0.491 m<sup>2</sup>/g, respectively.
- (3) The fractal dimensions obtained from LTNS and NMR exhibit strong consistency. The surface fractal dimensions ( $D_{L1}$  and  $D_{N1}$ ) increased with the increase in the number of hydraulic stimulation cycles, while the volume fractal dimensions ( $D_{L2}$  and  $D_{N2}$ ) exhibit an opposite trend to the surface fractal dimensions. The result indicates that, after the coal samples treated with CHS, the pore surface roughness and pore structure connectivity are both increased.
- (4) In the case of coal samples treated with CHS, both Langmuir volume and Langmuir pressure significantly decrease, consistent with the trend of TSSA change. The increments of Langmuir volume and Langmuir pressure ( $\Delta V_L$  and  $\Delta P_L$ ) exhibit a strong negative correlation with the increments of surface fractal dimensions ( $\Delta D_{L1}$  and  $\Delta D_{N1}$ ), indicating that the surface fractal dimensions can serve as an important parameter reflecting the changes in methane sorption characteristics for coal.

#### **CRediT authorship contribution statement**

**Rui-Shuai Ma:** Writing — original draft, Data curation. **Ji-Yuan Zhang:** Writing — review & editing, Investigation. **Qi-Hong Feng:** Writing — review & editing, Validation, Funding acquisition. **Xue-Ying Zhang:** Investigation, Data curation. **Yan-Hui Yang:** Formal analysis.

### **Declaration of competing interest**

The authors declare that they have no known competing financial interests or personal relationships that could have appeared to influence the work reported in this paper.

#### Acknowledgments

This study was financially supported by the National Natural Science Foundation of China (51904319) and the Fundamental Research Funds for the Central Universities (21CX06029A).

### Appendix A

Fig. A1 shows the results of  $T_2$  spectra of all the prepared raw coal samples, the abandoned and selected coal samples were marked by black and red solid lines, respectively. It can be seen from Fig. A1 that the  $T_2$  spectra of the selected coal samples are almost identical, and the positions of the three peaks are only slightly different. The similarity in  $T_2$  spectra indicates that the selected samples have similar pore structures, which means that the individual heterogeneity of the selected sample is insignificant, and the influence of individual sample differences on the NMR results can be ignored.

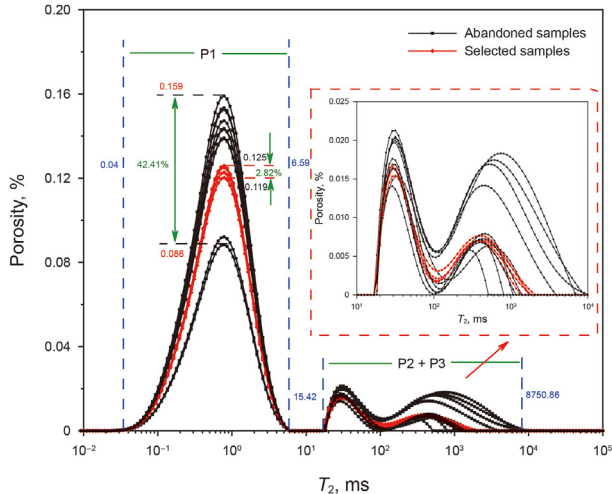


**Fig. A1.**  $T_2$  spectra of the cylindrical coal samples.

# Appendix B

In this section, the pore surface, pore volume and  $T_2$  spectra of the CHS untreated coal samples were selected to calculate the  $T_{2LM}$  and  $\rho$  based on the following equations (Tian et al., 2019; Zhai et al., 2022):

$$\rho = \frac{V}{ST_{2LM}} \tag{B1}$$

$$T_{2LM} = \exp\left[\sum_{i=1}^{n} \left(A_i \frac{\ln T_{2i}}{A_T}\right)\right]$$
 (B2)

where  $\rho$  is the surface relaxation rate, nm/ms;  $F_{\rm S}$  is the pore shape factor; V and S are the pore volume and pore surface area, which can be obtained by LTNS test, cm³/g and m²/g;  $T_{\rm 2LM}$  is the logarithmic mean of the transverse relaxation time, ms;  $A_i$  is the value of porosity at the point i, which can be obtained from NMR, %;  $T_{\rm 2i}$  is the value of  $T_{\rm 2}$  at the point i, ms;  $A_{\rm T}$  is the total porosity obtained from NMR, %.

From Table B1, it can be found that for coal samples with similar  $T_2$  spectra, there is little difference in the calculated results of  $\rho$ . In this study, the average value of the calculated results for  $\rho$  was selected to calculate the full-scale PSD.

**Table B1** Calculation of  $T_{\rm 2LM}$  and  $\rho$  of coal samples before CHS treatment.

Sample No.	Total pore volume, $10^{-3} \text{ cm}^3/\text{g}$	Total specific surface area, $10^{-2}$ m <sup>2</sup> /g	$T_{\rm 2LM}$ , ms	ρ, nm/ms	$\overline{ ho}$ , nm/ms
1	7.33	63.62	0.645	17.87	17.98
2			0.639	18.03	
3			0.642	17.95	
4			0.637	18.09	

#### References

- AlTammar, M., Sharma, M.M., 2019. Effect of borehole pressurization scheme on breakdown pressure. Rock Mech. Rock Eng. 52, 2709–2715. https://doi.org/ 10.1007/s00603-018-1731-7.
- Brunauer, S., Emmett, P., Teller, E., 1938. Absorption of gases in multimolecular layers. J. Am. Chem. Soc. 60, 309–319. https://doi.org/10.1021/ja01269a023.
- Bush, A., Gensterblum, Y., 2011. CBM and CO<sub>2</sub>-ECBM related sorption processes in coal: a review. Int. J. Coal Geol. 87, 49–71. https://doi.org/10.1016/ j.coal.2011.04.011.
- Cao, D.Y., Ning, S.Z., Guo, A.J., et al., 2016. Basic characteristics of coalfield tectonic framework in China. J. Min Sci. Technol. 1 (1), 1–8+10, 19606/ j.cnki.jmst.2016.01.002 (in Chinese).
- Chen, S., Tang, D., Tao, S., Xu, H., Li, S., Zhao, J., Jiang, Q., Yang, H., 2017. Pore structure characterization of different rank coals using N<sub>2</sub> and CO<sub>2</sub> adsorption and its effect on CH<sub>4</sub> adsorption capacity: a case in Panguan syncline, western Guizhou, China. Energy Fuels. 31, 6034–6044. https://doi.org/10.1021/acs.energyfuels.7b00675.
- Chen, X.J., Zhang, R.S., Zhao, X.B., et al., 2023. Multifractal estimation of NMR T<sub>2</sub> cutoff value in low-permeability rocks considering spectrum kurtosis: SMOTEbased oversampling integrated with machine learning. Petrol. Sci. 20 (6), 3411–3427. https://doi.org/10.1016/j.petsci.2023.08.001.
- Cheng, W.M., Liu, Z., Yang, H., et al., 2018. Non-linear seepage characteristics and influential factors of water injection in gassy seams. Exp. Therm. Fluid Sci. 91, 41–53. https://doi.org/10.1016/j.expthermflusci.2017.10.002.
- Clarkson, C., Solano, N., Bustin, R., et al., 2013. Pore structure characterization of North American shale gas reservoirs using USANS/SANS, gas sorption, and mercury intrusion. Fuel 103, 606–616. https://doi.org/10.1016/ i.fuel.2012.06.119.
- DiStefano, V.H., McFarlane, J., Stack, A.G., et al., 2019. Solvent-pore interactions in the Eagle Ford shale formation. Fuel 238, 298–311. https://doi.org/10.1016/i.fuel.2018.10.010.
- Fu, H.J., Tang, D.Z., Xu, T., et al., 2017. Characteristics of pore structure and fractal dimension of low-rank coal: a case study of Lower Jurassic Xishanyao coal in the southern Junggar Basin, NW China. Fuel 193, 254–264. https://doi.org/10.1016/ i.fuel.2016.11.069.
- Gaucher, E., Schoenball, M., Heidbach, O., et al., 2015. Induced seismicity in geothermal reservoirs: a review of forecasting approaches. Renewable Sustainable Energy Rev. 52, 1473—1490. https://doi.org/10.1016/j.rser.2015.08.026.
- Han, L.B., Wei, X.L., Zhang, J.C., 2022. Influence of structural damage on evaluation of microscopic pore structure in marine continental transitional shale of the Southern North China Basin: a method based on the low-temperature N<sub>2</sub> adsorption experiment. Petrol. Sci. 19 (1), 100–115. https://doi.org/10.1016/ i.petsci.2021.10.016.
- Hodot, B.B., 1961. Coal and Gas Outburst. China Industry Press, Beijing (in Chinese).
   Hu, B., Cheng, Y.P., Pan, Z.J., 2023. Classification methods of pore structures in coal: a review and new insight. Gas Sci. Eng. 110, 204876. https://doi.org/10.1016/

j.jgsce.2023.204876.

- Huang, Q.M., Liu, S.M., Wang, G., et al., 2019. Gas sorption and diffusion damages by guar-based fracturing fluid for CBM reservoirs. Fuel 251, 30—44. https://doi.org/ 10.1016/j.fuel.2019.04.031.
- Ji, Y.L., Yoon, J.S., Zang, A., et al., 2021. Mitigation of injection-induced seismicity on undrained faults in granite using cyclic fluid injection: a laboratory study. Int. J. Rock Mech. Min. Sci. 146, 104881. https://doi.org/10.1016/j.ijrmms.2021.104881.
- Laxminarayana, C., Crosdale, P., 1999. Role of coal type and rank on methane sorption characteristics of Bowen Basin, Australia coals. J. Int. J. Coal Geol. 40, 309–325, https://doi.org/10.1016/S0166-5162(99)00005-1.
- Lee, K., Ellsworth, W., Giardini, D., et al., 2019. Managing injection-induced seismic risks. Science 364 (6442), 730–732. https://doi.org/10.1126/science.aax18.
- Li, A., Ding, W.L., Jiu, K., Wang, Z., Wang, R., He, J., 2018. Investigation of the pore structures and fractal characteristics of marine shale reservoirs using NMR experiments and image analyses: a case study of the Lower Cambrian Niutitang Formation in northern Guizhou Province, South China. Mar. Petrol. Geol. 89, 530–540. https://doi.org/10.1016/j.marpetgeo.2017.10.019.
- Li, H., Kang, J., Zhou, F., Qiang, Z., Li, G., 2018. Adsorption heat features of coalbed methane based on microcalorimeter. J. Loss Prev. Process. Ind. 55, 437–449. https://doi.org/10.1016/j.jlp.2018.05.006.
- Li, H., Cao, J., Lu, J., Lin, B., Yu, Y., Shi, S., et al., 2024a. Effect of microwave-assisted cyclic oxidation on the coal internal and surface structure based on NMR and AFM. Energy 288, 129872. https://doi.org/10.1016/j.energy.2023.129872.
- Li, H., Lv, X., Lu, J., Liu, M., Yang, W., Hong, Y., et al., 2024b. Effect of cyclic thermal stimulation on the pore structure and fluid space of coal and inspiration for coalbed methane production. Energy 289, 129994. https://doi.org/10.1016/i.energy.2023.129994.
- Li, Y., Ning, F.L., Xu, M., et al., 2023. Experimental study on solid particle migration and production behaviors during marine natural gas hydrate dissociation by depressurization. Petrol. Sci. 20 (6), 3610–3623. https://doi.org/10.1016/j.petsci.2023.05.018.
- Liang, S., Liang, Y.W., Elsworth, D., et al., 2023. Permeability evolution and production characteristics of inclined coalbed methane reservoirs on the southern margin of the Junggar Basin, Xinjiang, China. Int. J. Rock Mech. Min. Sci. 171, 105581. https://doi.org/10.1016/ji.ijrmms.2023.105581.
- Liu, T., Zhai, C., Zhao, Y., et al., 2021. Evaluation on stress sensitivity of multiscale pore and fracture in shale based on LF NMR. J. China Coal Soc. 46 (S2), 887–897. https://doi.org/10.13225/j.cnki.jccs.2021.0852 (in Chinese).
- Mohanty, M.M., Kumar, B., 2017. Sorption behavior of coal for implication in coal bed methane an overview. Int. J. Min. Sci. Technol. 27, 307—314. https://doi.org/10.1016/j.ijmst.2017.01.014.
- Ni, G.H., Dong, K., Li, S., et al., 2019. Gas desorption characteristics effected by the pulsating hydraulic fracturing in coal. Fuel 236, 190–200. https://doi.org/ 10.1016/i.fuel.2018.09.005.
- Niemz, P., Cesca, S., Heimann, S., et al., 2020. Full-waveform-based characterization of acoustic emission activity in a mine-scale experiment: a comparison of conventional and advanced hydraulic fracturing schemes. Geophys. J. Int. 222, 189–206. https://doi.org/10.1093/gji/ggaa127.
- Ozdemir, E., 2016. Role of pH on CO<sub>2</sub> sequestration in coal seams. Fuel 172, 130—138. https://doi.org/10.1016/j.fuel.2016.01.021.
- Patel, S.M., Sondergeld, C.H., Rai, C.S., 2017. Laboratory studies of hydraulic fracturing by cyclic injection. Int. J. Rock Mech. Min. Sci. 95, 8–15. https://doi.org/10.1016/j.ijrmms.2017.03.008.
- Pfeifer, P., Wu, Y., Cole, M., et al., 1989. Multilayer sorption on a fractally rough surface. Phys. Rev. Lett. 62, 1997–2000. https://doi.org/10.1103/PhysRevLett.62.1997.
- Pyun, S.I., Rhee, C.K., 2004. An investigation of fractal characteristics of mesoporous carbon electrodes with various pore structures. Electrochim. Acta 49 (24), 4171–4180. https://doi.org/10.1016/j.electacta.2004.04.012.
- Rutqvist, J., Birkholzer, J., Cappa, F., et al., 2007. Estimating maximum sustainable injection pressure during geological sequestration of CO<sub>2</sub> using coupled fluid flow and geomechanical fault-slip analysis. Energy Convers. Manag. 48 (6), 1798–1807. https://doi.org/10.1016/j.enconman.2007.01.021.
- Senthamaraikkannan, G., Gates, G., Prasad, V., 2016. Multiphase reactive-transport simulations for estimation and robust optimization of the field scale production of microbially enhanced coalbed methane. Chem. Eng. Sci. 149, 63–77. https://doi.org/10.1016/j.ces.2016.04.017.
- Shao, X.H., Pang, X.Q., Li, H., et al., 2017. Fractal analysis of pore network in tight gas sandstones using NMR method: a case study from the Ordos basin, China. Energy Fuels. 31 (10), 10358–10368. https://doi.org/10.1021/acs.energyfuels.7b01007.
- Sing, K., 1985. Reporting physisorption data for gas/solid systems with special reference to the determination of surface area and porosity (Recommendations 1984). Pure Appl. Chem. 57 (4), 603–619. https://doi.org/10.1351/pac198557040603.
- Su, E.L., Liang, Y.P., Zou, Q.L., 2021. Structures and fractal characteristics of pores in long-flame coal after cyclical supercritical CO<sub>2</sub> treatment. Fuel 286, 119305. https://doi.org/10.1016/j.fuel.2020.119305.
- Su, X., Li, F., Su, L., Wang, Q., 2020. The experimental study on integrated hydraulic fracturing of coal measures gas reservoirs. Fuel 270, 117527. https://doi.org/ 10.1016/j.fuel.2020.117527.
- Sudibandriyo, M., Pan, Z.J., Fitzgerald, J., et al., 2003. Sorption of methane, nitrogen, carbon dioxide, and their binary mixtures on dry activated carbon at 318.2 K and pressures up to 13.6 MPa. Langmuir 19 (13), 5323–5331. https://doi.org/10.1021/la020976k.

- Sun, X., Zhou, H., Xue, D., et al., 2021. Experimental study of spontaneous imbibition of low-permeability coal based on NMR. J. China Univ. Min. Technol. 50 (4), 804–812. https://doi.org/10.13247/j.cnki.jcumt.001321 (in Chinese).
- Tang, J.P., Qi, T., Dai, S., et al., 2020. Experimental study on hydraulic fracturing effects of horizontal stress difference on cyclic water injection stress transformation. Chin. J. Appl. Mech. 37 (3), 990–998 (in Chinese) doi:10.11776/ cjam.37.03.B027.
- Tao, S., Pan, Z.J., Tang, S.L., et al., 2019. Current status and geological conditions for the applicability of CBM drilling technologies in China: a review. Int. J. Coal Geol. 202, 95–108. https://doi.org/10.1016/j.coal.2018.11.020.
- Tian, W., Lu, S., Huang, W., et al., 2019. Study on the full-range pore size distribution and the movable oil distribution in glutenite. Energy Fuels. 33 (8), 7028–7042. https://doi.org/10.1021/acs.energyfuels.9b00999.
- Velcin, H., Dautriat, J., Sarout, J., et al., 2020. Experimental reactivation of shear-fractured Berea and Boise sandstones by brine or liquid CO<sub>2</sub> injection at depth. J. Geophys. Res. B Solid Earth Planets 125 (2), e2019JB018281. https://doi.org/10.1029/2019JB018281
- Wang, J., Guo, S.B., 2021. Study on the relationship between hydrocarbon generation and pore evolution in continental shale from the Ordos Basin, China. Petrol. Sci. 18, 1305–1322. https://doi.org/10.1016/j.petsci.2021.01.002.
- Wang, W.C., Li, X.Z., Lin, B.Q., et al., 2015. Pulsating hydraulic fracturing technology in low permeability coal seams. Int. J. Min. Sci. Technol. 25 (4), 681–685. https://doi.org/10.1016/j.ijmst.2015.05.025.
- Xue, S., Huang, Q.M., Wang, G., et al., 2021. Experimental study of the influence of water-based fracturing fluids on the pore structure of coal. J. Nat. Gas Sci. Eng. 88, 103863. https://doi.org/10.1016/j.jngse.2021.103863.
- Yang, K., Zhou, J.P., Xian, X., et al., 2023. Effect of supercritical CO<sub>2</sub>-water-shale interaction on mechanical properties of shale and its implication for carbon sequestration. Gas Sci. Eng. 111, 204930. https://doi.org/10.1016/j.jgsce.2023.204930.
- Yang, Y., Liu, S., Zhao, W., Wang, L., 2019. Intrinsic relationship between Langmuir sorption volume and pressure for coal: experimental and thermodynamic

- modeling study. Fuel 241, 105–117. https://doi.org/10.1016/j.fuel.2018.12.008.
- Yao, Y., Liu, D.M., Tang, D.Z., et al., 2008. Fractal characterization of sorption-pores of coals from North China: an investigation on CH<sub>4</sub> sorption characteristic of coals. Int. J. Coal Geol. 73, 27–42. https://doi.org/10.1016/j.coal.2007.07.003.
- Yin, G.J., Liu, Q.Y., Liu, Z.Y., et al., 2018. Extension of Kelvin equation to CO<sub>2</sub> sorption in activated carbon. Fuel Process. Technol. 174, 118—122. https://doi.org/10.1016/ i.fuproc.2018.02.006.
- Yuan, Y., Rezaee, R., 2019. Fractal analysis of the pore structure for clay bound water and potential gas storage in shales based on NMR and N<sub>2</sub> gas sorption. J. Petrol. Sci. Eng. 177, 756–765. https://doi.org/10.1016/j.petrol.2019.02.082.
- Zhai, C., Sun, Y., Fan, Y., et al., 2022. Application and prospect of low-filed nuclear magnetic resonance technology in accurate characterization of coal pore structure. J. China Coal Soc. 47 (2), 828–848. https://doi.org/10.13225/j.cnki.jccs.xr21.1766 (in Chinese).
- Zhang, T.T., Li, Z.P., Adenutsi, C.D., et al., 2022. Quantitative investigation of nanofluid imbibition in tight oil reservoirs based on NMR technique. Petrol. Sci. 19, 2185–2198. https://doi.org/10.1016/j.petsci.2022.04.013.
- Zhao, J., Xu, H., Tang, D., Mathews, J.P., Li, S., Tao, S., 2016. A comparative evaluation of coal specific surface area by CO<sub>2</sub>, and N<sub>2</sub>, adsorption and its influence on CH<sub>4</sub>, adsorption capacity at different pore sizes. Fuel 183, 420–431. https://doi.org/10.1016/j.fuel.2016.06.076
- Zheng, S.J., Yao, Y.B., Liu, D.M., et al., 2019. Nuclear magnetic resonance surface relaxivity of coals. Int. J. Coal Geol. 205, 1–13. https://doi.org/10.1016/i.coal.2019.02.010.
- Zhou, H., Liu, Z., Sun, X., Ren, W., Zhong, J., Zhao, J., Xue, D., 2021. Evolution characteristics of seepage channel during water infusion in deep coal samples. J. China Coal Soc. 46, 867–875. https://doi.org/10.13225/j.cnki.jccs.yt20.1966 (In Chinese).
- Zhou, J.P., Yang, K., Tian, S., et al., 2020. CO<sub>2</sub>-water-shale interaction induced shale microstructural alteration. Fuel 263, 116642. https://doi.org/10.1016/j.fuel.2019.116642.